PROPAGATION OF NEURONAL ACITVITY BY ELECTRIC FIELD

by

CHEN QIU

Submitted in partial fulfillment of the requirements

for the degree of Master of Science

Department of Biomedical Engineering

CASE WESTERN RESERVE UNIVERSITY

May, 2014

CASE WESTERN RESERVE UNIVERSITY

SCHOOL OF GRADUATE STUDIES

We hereby approve the thesis/dissertation of

Chen Qiu

candidate for the degree of **Master of Science***.

Committee Chair

Dr. Dominique Durand

Committee Member

Dr. Hillel Chiel

Committee Member

Dr. Kenneth Gustafson

Date of Defense

2/25/2014

*We also certify that written approval has been obtained

for any proprietary material contained therein.

Dedication

For my dear mama and baba- Shumei and Yan Qiu

Thank you for letting me be myself

I love you

For my sisters and brothers at the Church in Cleveland

Through your unceasing prayers, I turned my head to God

In Him was Life, and that Life was the light of men.

John 1:4

TABLE OF CONTENTS

LIST OF TABLES

LIST OF FIGURES

Acknowledgements

I would like to thank my advisor and mentor, Dr. Dominique Durand, for his passion, enthusiasm, and ethics toward biomedical research that greatly influenced me to become a professional scientist and engineer; his constantly impressive ideas that inspired my innovative thinking during our brainstorming sessions; and his patience and support on my academic and personal achievements during both my undergraduate and graduate years. My thesis committee members, Dr. Kenneth Gustafson and Dr. Hillel Chiel, who taught me everything I needed in the area of bioelectrical engineering and neurosciences that allowed me to finish this work. They all have encouraged me so much to accomplish more than what I thought I could do.

To my colleagues in the lab at Neural Engineering Center, Mingming, who helped me understand the goals of this research work by demonstrating his experiments and actively discussing with me, and whose experimental results served as a strong validation for my simulation model; Rajat, Luis, and Jesse, for our interesting and sometimes frustrating discussions and debate on the “beauty” of field effect; Tom, Sheela, and David, for your constant encouragement, kindness, and support whenever I fell into tough situations.

To my parents, for not only supporting me on every dream I wanted to achieve, but also treating me as peer whenever we discuss science and research- I feel proud that everyone in the family is in the STEM field and I have continued that tradition. To my church sisters and brothers, without you, I wouldn’t know who I am and what I want.

Thank you all. This is for you.

PROPAGATION OF NEURONAL ACITVITY BY ELECTRIC FIELD

Abstract

by

Chen Qiu

The propagations of several types of neuronal activity such as theta wave or epilepsy exhibit a similar speed of approximately 0.1m/s with or without synapses, suggesting that there exists a shared non-synaptic governing mechanism. Electrical field effect is a potential candidate, as it is known to modulate spiking patterns and timing. Here, we develop a simulated CA1 pyramidal network with cells connected solely through field effect and test the hypothesis that electric field alone is responsible for neuronal activity propagation. Results show that field effect can mediate the transverse propagation with a speed of 0.12 ± 0.097 m/s upon spiking initiation with simulated field amplitudes of 3-6mV/mm, similar to that observed physiologically. We also showed an inverse relationship between osmolarity and propagation speed, both in mouse hippocampal slices and simulation. We conclude that, despite its weak amplitude, field effect can be responsible for neuronal activity propagation.

CHAPTER 1

INTRODUCTION AND HYPOTHESES

1.1 INTRODUCTION

1.1.1 Neuronal Activity Propagation and Relative Mechanisms

The brain is a highly modular structure where rhythmic or repetitive neural oscillation exists throughout the neural tissue. Even though the brain is densely packed with neurons, only a very small fraction of them are activated in response to a stimulus or in a cognitive or motor task [1], while the rest are activated through the spiking activity propagation. In general, such oscillations can be characterized by their frequency/amplitude (theta, gamma, etc.) or their spiking patterns (bursting, sharp wave-ripple complexes, etc.), and can be usually monitored by electroencephalogram (EEG), electronystagmogram (ENG), electromyogram (EMG), and glass pipettes or electrode arrays on small scale experiments. The functions of neuronal propagations are wide ranging. Under normal conditions, neuronal activity propagation is crucial for many neural functions such as motor coordination, perception, memory, and consciousness. In addition, specific types of neural oscillations also appear in pathological situations such as tremor or epilepsy, characterized by involuntary or excessive spiking travelling [2], [3]. Thus, to understand how to control and modulate the essential cognitive and motor functions or to understand pathological conditions related to neuronal oscillations, it is

essential to identify the conditions under which each corresponding type of neuronal activity propagation can proceed.

The mechanisms for neuronal propagation can be understood by examining how neurons communicate among one another. Chemical synaptic transmission is the most well-known mechanism that links the membranes of two adjacent neurons together and carries out the signaling process. Specifically, electrical activity in presynaptic cells is converted into the release of neurotransmitters that bind to postsynaptic receptors and initiate electrical responses in the postsynaptic cells. Electrical synapses (gap junctions) are composed of two connexin proteins and form a narrow channel that directly connect the two cells and allow electrical coupling [4]. Although synaptic transmission is clearly the most important way for neural to communicate, non-synaptic mechanisms have been proven to either allow or affect the transmission of electrical signals among cells. Ionic diffusive coupling were shown to cause seizure-like activity to propagate with a slow speed [5], [6], [7], [8] whereby ions diffuse from one cell to its neighbor and can change excitability of the cell [9]. Endogenous or applied electrical fields can also affect neuronal firing and interaction due to the change of membrane polarization. Despite their small size, these fields are able to entrain action potentials and affect neural functions under physiological conditions [10]. However, they have not been implicated in the propagation of neural activity.

1.1.2 Mechanism and Functions of Electrical Field Effect

Electrical fields can indirectly affect neuronal excitability by modulating the membrane voltage.Also known as ephaptic effect (or coupling), it was first discovered

and demonstrated in 1940 by Katz and Schmitt. They experimented on the limb nerve of a crab “Carcinus maenas” and showed that one excited non-myelinated nerve could affect the excitability of another non-myelinated nerve, when these two nerves were in parallel and isolated [11]. The electric field effect mostly occurs locally, when a change in electrical activity at certain location of one cell creates a dipole (or a local circuit thus the extracellular electrical field) that acts as a virtual extracellular stimulation to cells nearby and in turn influences their neuronal activity (Fig. 1.1). Electrical field effect was found to occur anywhere in a cell such as axon to axons [12], somas [10], and even within chemical synaptic clefts where Ca^{2+} channels are affected by the local field [13]. The central structures that exhibit field effects were found in hippocampus, spinal cord, cortex, olfactory bulbs, retina, and peripheral auditory nervous system [12], [14].

The significances of electrical field effect under different settings and locations are diverse, and the mechanism has attracted research interests on its impact on neuronal activity generation, synchronization, and modulation. There have been numerous studies employing externally applied weak fields to polarize neurons, and the field effect was shown to have both excitatory and inhibitory-effects at various degrees. A recent study has shown that field effect could strongly entrain action potential timing, particularly for slow fluctuations of the extracellular field, although the field only mediate very small changes in somatic membrane potential [10]. Furthermore, during concurrent to suprathreshold synaptic input, the spike timing change was shown to have a linear dependency on field strength for low-frequency fields, and the mean firing phase and coherence of the spiking each increased monotonically with field strength for high-frequency fields [15]. Computational simulation studies also validated that field effect

can greatly affect spike timing [10] and can lead to synchronization of independently firing neurons [12]. On the contrary, electrical field may also have inhibitory effect within chemical synapses, such as in mammalian cerebellum, where a strong barrier exists to current flow causing an opposite flow direction and a transient electrical hyperpolarization [16].

Research studies on the topic of electrical field effect suggested that despite its weak amplitude recorded under physiological or pathological conditions (around 1-5mV/mm, [10], [15], [17]), the electrical field has a significant role in neuronal activity modulation. However, thus far, most experimental and computation studies have focused on how externally applied DC or simulated field waveform (sinusoidal) affect single neurons and none has mentioned the role of field effect on neuronal activity propagation within a cellular network. Francis et al. suggests that a cellular network is more sensitive to weak fields than individual cell [17]. Recently, it has been suggested that electric field are responsible for the propagation of epileptiform activity in the hippocampus after diffusion, electrical, and chemical mechanisms were eliminated [18]. It is difficult, however, to directly show that electrical fields are responsible in experimental settings. Here, we take the advantage of computer simulation to determine if electrical fields alone can be responsible for the neuronal activity propagation.

1.2 STATEMENT OF RESEARCH HYPOTHESES

The primary goal of this study is to investigate whether, upon neuronal activity initiation, the network endogenous electrical field effect alone is sufficient to drive *propagation* of the activity within the neuronal network itself. The study is conducted through computational simulation of a hippocampal CA1 pyramidal cellular network that is connected by no other means but field effect interaction and validated by experimental data. The specific objectives and hypotheses of the study are:

(I) To develop a computational model of a transverse cellular network containing hippocampal CA1 pyramidal neurons that are isolated and can be only affected by electrical field created by their adjacent cells, and that the cellular volume density in the network is physiological.

(II) To study whether, upon initiation of spiking activities in the cells of the first row, that the activity can propagate through the rest of the cells in the network. We hypothesize that *electrical field effect solely can drive the propagation of neuronal activity within a cellular network.*

(III) To record the speed and the network field amplitude during propagation (if propagation occurs), and compare the values to those observed experimentally. We hypothesize that *the neuronal activity propagation governed by electrical field effect exhibits a speed of 0.1m/s regardless of whether it is under normal or pathological conditions.*

(IV) To study the effect of osmolarity on network field amplitude and its relationship with the neuronal activity propagation speed (if propagation occurs), validated by

experimental measurements. We hypothesize that the extracellular volume is inversely related to the propagation speed.

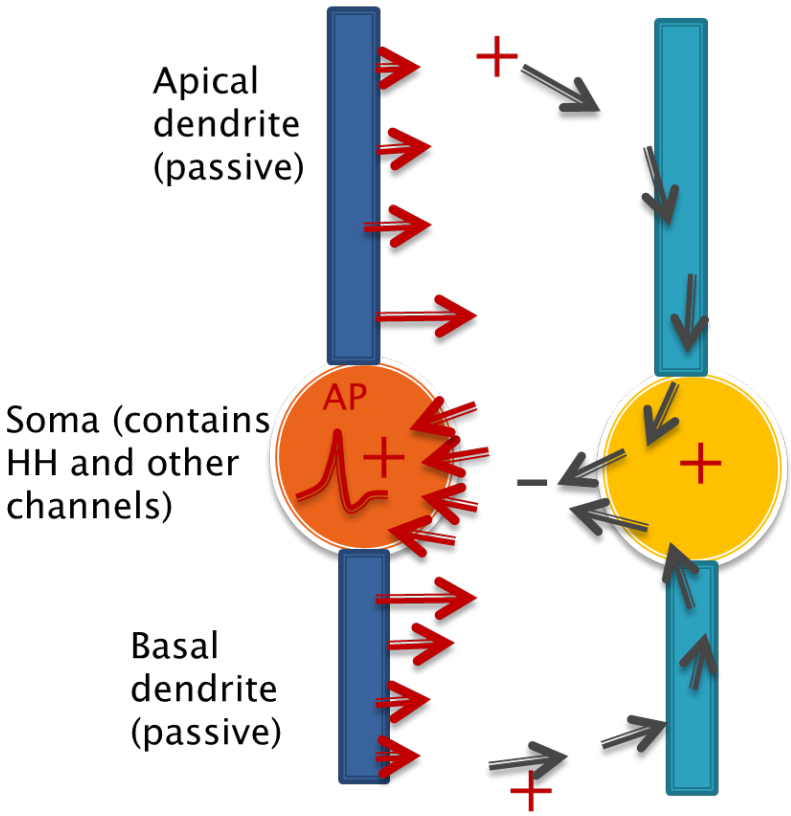

Figure 1.1. Graphical demonstration of electrical field effect for cell to cell interaction. When an action potential occurs at the soma, current flows into the soma and out at the dendrites, creating a local current loop. This loop will in turn depolarize the adjacent neuron that was originally at rest and modulate its electrical activity.

1.3 REFERENCES

[1] A. Kumar, S. Rotter, and A. Aertsen, “Spiking activity propagation in neuronal networks: reconciling different perspectives on neural coding,” *Nat. Rev. Neurosci.*, vol. 11, no. 9, pp. 615–627, Sep. 2010.

[2] J. H. McAuley and C. D. Marsden, “Physiological and pathological tremors and rhythmic central motor control,” *Brain*, vol. 123, no. 8, pp. 1545–1567, Aug. 2000.

[3] V. Shusterman and W. C. Troy, “From baseline to epileptiform activity: a path to synchronized rhythmicity in large-scale neural networks,” *Phys. Rev. E Stat. Nonlin. Soft Matter Phys.*, vol. 77, no. 6 Pt 1, p. 061911, Jun. 2008.

[4] J. R. Gibson, M. Beierlein, and B. W. Connors, “Functional Properties of Electrical Synapses Between Inhibitory Interneurons of Neocortical Layer 4,” *J. Neurophysiol.*, vol. 93, no. 1, pp. 467–480, Aug. 2004.

[5] A. Konnerth, U. Heinemann, and Y. Yaari, “Nonsynaptic epileptogenesis in the mammalian hippocampus in vitro. I. Development of seizurelike activity in low extracellular calcium,” *J. Neurophysiol.*, vol. 56, no. 2, pp. 409–423, Aug. 1986.

[6] F. Weissinger, K. Buchheim, H. Siegmund, U. Heinemann, and H. Meierkord, “Optical imaging reveals characteristic seizure onsets, spread patterns, and propagation velocities in hippocampal-entorhinal cortex slices of juvenile rats,” *Neurobiol. Dis.*, vol. 7, no. 4, pp. 286–298, Aug. 2000.

[7] J. Lian, M. Bikson, J. Shuai, and D. M. Durand, “Propagation of non-synaptic epileptiform activity across a lesion in rat hippocampal slices,” *J. Physiol.*, vol. 537, no. Pt 1, pp. 191–199, Nov. 2001.

[8] D. M. Durand, E.-H. Park, and A. L. Jensen, “Potassium diffusive coupling in neural networks,” *Philos. Trans. R. Soc. B Biol. Sci.*, vol. 365, no. 1551, pp. 2347–2362, Jul. 2010.

[9] K. Bar-Eli, “Coupling of chemical oscillators,” *J. Phys. Chem.*, vol. 88, no. 16, pp. 3616–3622, Aug. 1984.

[10] C. A. Anastassiou, R. Perin, H. Markram, and C. Koch, “Ephaptic coupling of cortical neurons,” *Nat. Neurosci.*, vol. 14, no. 2, pp. 217–223, Jan. 2011.

[11] B. Katz and O. H. Schmitt, “Electric interaction between two adjacent nerve fibres,” *J. Physiol.*, vol. 97, no. 4, pp. 471–488, Feb. 1940.

[12] H. Bokil, N. Laaris, K. Blinder, M. Ennis, and A. Keller, “Ephaptic interactions in the mammalian olfactory system,” *J. Neurosci. Off. J. Soc. Neurosci.*, vol. 21, no. 20, p. RC173, Oct. 2001.

[13] M. Kamermans and I. Fahrenfort, “Ephaptic interactions within a chemical synapse: hemichannel-mediated ephaptic inhibition in the retina,” *Curr. Opin. Neurobiol.*, vol. 14, no. 5, pp. 531–541, Oct. 2004.

[14] D. S. Faber and H. Korn, “Electrical field effects: their relevance in central neural networks,” *Physiol. Rev.*, vol. 69, no. 3, pp. 821–863, Jul. 1989.

[15] T. Radman, Y. Su, J. H. An, L. C. Parra, and M. Bikson, “Spike timing amplifies the effect of electric fields on neurons: implications for endogenous field effects,” *J. Neurosci. Off. J. Soc. Neurosci.*, vol. 27, no. 11, pp. 3030–3036, Mar. 2007.

[16] H. Korn and H. Axelrad, “Electrical inhibition of Purkinje cells in the cerebellum of the rat,” *Proc Natl Acad Sci USA*, vol. 77, no. 10, pp. 6244–6247, Oct. 1980.

[17] J. T. Francis, B. J. Gluckman, and S. J. Schiff, “Sensitivity of neurons to weak electric fields,” *J. Neurosci. Off. J. Soc. Neurosci.*, vol. 23, no. 19, pp. 7255–7261, Aug. 2003.

[18] M. Zhang, T. P. Ladas, C. Qiu, R. S. Shivacharan, L. E. Gonzalez-Reyes, and D. M. Durand, “Propagation of epileptiform activity can be independent of synaptic transmission, gap junctions, or diffusion and is consistent with electrical field transmission,” *J. Neurosci. Off. J. Soc. Neurosci.*, vol. 34, no. 4, pp. 1409–1419, Jan. 2014.

CHAPTER 2

PROPAGATION OF NEURONAL ACTIVITY BY ELECTRIC FIELD

2.1 INTRODUCTION

Electrical signal propagation is one of the properties in a neuronal network that enables communications among neurons. In the hippocampus, such communication is essential for basic neural function such as memory, or, if abnormal, can cause pathological conditions such as epilepsy. In particular, the propagation of epileptiform activity has been intensively researched in various epilepsy models, as well as the propagation of theta oscillations during awake behavior and rapid eye movement (REM) sleep [1]. Surprisingly, the propagation speeds of these two types of activity are very similar. Epileptiform events generated by 4-aminopyridine (4-AP) travel with a longitudinal speed of 0.09±0.03 m/s along the CA3 region [2]. Similarly, in the presence of picrotoxin, synchronous firing events propagate longitudinally at 0.14±0.04 m/s [3]. Ionic concentration changes in ACSF also triggers epileptiform activity, and in high K^+, low Mg^{2+}, and low Ca^{2+} induced models, either in transverse slices or whole hippocampus, speeds of 0.07 to 0.1m/s [4], 0.1 to 0.15m/s [5], and 0.04 to 0.15m/s [6] were observed, respectively. In normal tissue, theta oscillations travel with a speed of 0.87 to 0.107m/s in the hippocampus of living rodent rats [1], while carbachol-induced theta oscillations in transverse slices

exhibited a speed of 0.119 m/s along CA1 cell layer and a 0.141 m/s along CA3 cell layer [7]. Taken together, it is clear that both epileptiform activity and theta oscillations in hippocampus travel with a speed of approximately 0.1 m/s regardless of experimental models, and that a shared fundamental mechanism may exist underlying these neuronal propagations.

Despite the fact that chemically-mediated synaptic transmission and electrically-mediated gap junctions are generally known to be responsible for neuronal communication, these two mechanisms were not required during propagation, since neural activity could still travel at the same or even higher speed in the presence of synaptic blockers such as low Ca^{2+}/4-AP aCSF condition [6], [8], [9] and gap junction blockers such as mefloquine/4-AP aCSF condition [9]. Other propagation mechanisms such as extracellular ionic transients and axonal conduction mechanisms were reported to have very different propagation speed (0.0004 to 0.008m/s for K^{+}diffusion and 0.3 to 0.5m/s caused by axonal conduction, [3],[10], [11], [12], [13], [14]). Thus, it is unlikely that neuronal activity propagation at around 0.1m/s can be explained by synaptic transmission, gap junction, diffusion, or axonal propagation. The only other mechanism to explain such propagation is through electric field effects, as experiments have shown that extracellular field effect could modulate the activity of single neurons and/or network activity. In hippocampal pyramidal cells, weak electrical fields can modulate the excitability of cells and play a role in the synchronization of the network [15]. In cortical neurons, endogenous field with a similar amplitude could strongly entrain action potentials under physiological conditions and pharmacologically evoked network activity and lead to phase locking

of spikes to the external field to reach a “spike-field synchrony” [16], [17]. The fact that the cellular packing is relatively tight in certain brain regions increases the field interactions between cells [18]. Yet, electrical fields have not been thought to be involved in the propagation of neural activity. Thus, in this thesis, we test the hypothesis that an electrical field effect could cause neuronal activity to travel with a speed of 0.1m/s in hippocampus through a computational model that includes cells connected by no other means (such as synapses or gap junctions). The hippocampal CA1 pyramidal cellular network was tested, as it is a typical region where neuronal propagation was observed experimentally. Two experimental models were simulated - 4-AP/no [Ca^{2+}] condition and normal aCSF condition- in order to understand the scope and significance of electrical field effect in various types of neuronal propagation. We examined the propagation speed and resulting network field amplitude in the modeled cellular network and compared it with neural activity propagation patterns in *in-vitro* experiments. The model predictions related to the effect of packing density on propagation speed were confirmed by osmolarity experiments.

2.2 METHODS

2.2.1 Model structure

The neuronal CA1 hippocampal pyramidal network was built under the NEURON 7.3 simulation environment (Yale School of Medicine, New Haven, CT). In the model, each CA1 hippocampal pyramidal cell was constructed using a 3-D cylinder shape for dendrites and spherical shape for the soma that was located between the apical and basal dendritic cylinders. The morphology of each cell is shown in **Fig. 2.1** with 33-compartments, including one compartment for the soma, 21 compartments for the apical dendrite, and 11 compartments for the basal dendrite. The lengths of the apical and basal dendrites were 735.3 μm and 490.2 μm, respectively, while both had a diameter of 5.2 μm [19]. Similar as previous experiments and models, the diameter of each cell body was 10 μm [16], [19]-[20].

The transmembrane potential V_i for each compartment of the model is described by the relationship known as the cable equation **(Eq. 1)**.

$$C_{m,i}\frac{dV_i}{dt} = -I_{m,i} + r_{i,i+1}\left(V_{i+1} - V_i\right) + r_{i,i-1}\left(V_{i-1} - V_i\right) \quad \textbf{(1)}$$

where $C_{m,i}$, V_i, $I_{m,i}$, are the membrane capacitance, transmembrane potential, and transmembrane current of the i-th compartment respectively; $r_{i,i+1}$ is the cytoplasmic (axial) conductivity between the i -th and (i +1)-th compartment. In calcium-free solution, the calcium currents and calcium-dependent potassium currents are eliminated [19]. In addition, to simplify the model, only the soma compartment contains an active conductance; for dendritic compartments, the transmembrane current only contains leak

current $I_{m,i}^{dend} = I_{leak,i} = g_i V_i$, with g_i representing the passive conductance of the i -th compartment.

All passive membrane properties for each pyramidal cell were set to the following values according to patch clamp recordings and current clamp data in Ca^{2+} -free conditions by Shuai et al. 2003: somatic membrane resistivity $R_m^{soma} = 680\ \Omega \cdot cm^2$, somatic membrane capacitance $C_m^{soma} = 1.0\ \mu F/cm$, dendrite membrane resistivity $R_m^{dend} = 34{,}200\ \Omega \cdot cm^2$, dendritic capacitance $C_m^{dend} = 1.0\ \mu F/cm$, and cytoplasmic (axial) resistivity $R_i = 530\ \Omega \cdot cm$ [19].

2.2.2 Active ionic conductances

For each cell in the model, the transmembrane current for somatic compartments $I_{m,i}^{soma}$ are given by:

$$I_{m,i}^{soma} = I_{Leak,i} + I_{Ions,i} \quad \textbf{(2)}$$

where $I_{Leak,i}$ and $I_{Ions,i}$ are the leak current and total active ionic currents respectively. Previous *in-vitro* experiments and computational models for CA1 hippocampal pyramidal cell stated that there are generally five major active ionic conductances in a Ca-free extracellular environment: a fast sodium current I_{Na}, a delayed rectifier current I_{DR}, an A-type transient current I_A, a muscarinic current I_M, and a persistent sodium current I_{NaP} [19], [21]. Thus, the total ionic current in the somatic compartment consists of five active currents:

$$I_{Ions,i} = I_{Na} + I_{DR} + I_A + I_M + I_{NaP} \quad \textbf{(3)}$$

The gating equations for each active current are implemented using the Hodgkin-Huxley formalism [22] as follows:

$$I_{Na} = g_{Na} m^3 h \left(V_m - E_{Na}\right)$$

$$I_{NaP} = g_{NaP} w \left(V_m - E_{Na}\right)$$

$$I_{DR} = g_{DR} n^4 \left(V_m - E_K\right)$$

$$I_A = g_A ab \left(V_m - E_K\right)$$

$$I_M = g_M u^2 \left(V_m - E_K\right)$$

$$I_L = g_L \left(V_m - E_L\right) \qquad \textbf{(4a)}$$

The maximum conductance in Eq. 4a and b are based on those of Shuai et al. [19], where their established models reproduced the electrophysiological behavior of CA1 pyramidal cells in low Ca concentration environment. However, *in-vitro* experiments in our study were performed in an environment that also contained 4-aminopyridine (4-AP), a blocker of the Kv1 voltage-activated K^+ (A-type transient K) channels. Thus, we greatly reduced the maximum A channel conductance, g_A, to a near-zero value so to mimic the experimental model. In addition, the Hodgkin-Huxley Na channel maximum conductance g_{Na} was modified to the lowest value that allowed cells to fire with initial stimulation in the model, 0.048 S/cm^2, a value that is still lower than the largest physiological g_{Na} value reported for CA1 pyramidal cells, 0.15 S/cm^2 [21]. **Table 2.1** shows the maximum conductance values used in the model.

Each gate variable *x* (i.e. *m, h, w, n, a, b, u*) depends on its corresponding gate function,

$$\frac{dx}{dt} = \frac{x_\infty - x}{\tau_x} \qquad \textbf{(4b)}$$

where $x_\infty = \alpha_x/(\alpha_x + \beta_x)$ and $\tau_x = 1/(\alpha_x + \beta_x)$. The rate functions (α_x, β_x) for all currents were the same as those in Shuai et al. [19].

2.2.3 The neuronal network model

The layout of the CA1 neuronal network in the model was designed in a way to capture the most important features of the physiological cellular layout for hippocampal activity propagation while minimizing the number of elements. The network is made up of three rows (Row A, B, and C) of neurons with ten cell locations in each row **(Fig. 2.2 A and B)**. The distance between each two adjacent neurons in a physiological pyramidal network ranges from 2 to 5 μm [16], [20]; in the model, we tested cell-to-cell distance (d_{c-c}) equals 2, 3, and 4 μm (n=10 and variance=0.1μm with Gaussian distribution for each d_{c-c}). To represent the cell stacking throughout the depth of a tissue slice, an arbitrary "stacking factor" (SF) was generated to take into account the real number of cells around a certain location. An SF of 3 means that for every cell location in the network, there are three cells stacking around the same spot vertically throughout the depth of the slice **(Fig. 2.2 C)**. The value of the SF was estimated from the volume cellular density reported from previous histology studies. In mice hippocampus, CA1 cellular volume density varies from approximately 180,000 $\text{neurons}/mm^3$ to 300,000 $\text{neurons}/mm^3$ [20], [23] depending on specific locations in CA1 region. The thickness of a typical hippocampal slice is usually around 600 μm. With the model network area equals to approximately 4216 μm^2 to 4788 μm^2 (**Fig. 2.2 A**: $\bar{d}$=2 μm, area=34 μm× 124μm; $\bar{d}$=4 μm, area=38 μm× 136μm;), SF between 15 to 28 would best represent the

cellular layout in tissue. In the model, stacking factor values between 10 and 30 were tested.

2.2.4 *In-vitro* measurements (low Ca^{2+} /4-AP) of extracellular activity in hippocampus

In-vitro measurements of extracellular activity and electric field in mice hippocampus were performed to measure the propagation speed and validate the results of the simulation. Experimental protocols were approved by the Institutional Animal Case and Usage Committee. CD1 Mice from Charles River (P10-P20) were anesthetized and then decapitated. Subsequently, the whole hippocampus was separated from the brain and unfolded by following a previously developed protocol [12]. All unfolded hippocampal preparations were then transferred into a recovery solution of aCSF bubbled with 95% O_2/5% CO_2 and maintained at a room temperature (25^oC) for at least one hour before recording. Normal aCSF buffer consisted of (mM): NaCl 124, KCl 3.75, KH_2PO_4 1.25, $MgSO_4$ 2, $NaHCO_2$ 26, Dextrose 10 and $CaCl_2$ 2. 4-aminopyridine (4-AP), a blocker of the Kv1 voltage-activated K^+ channels, was used to increase the excitability of the tissue [24], [25], [26]. Low Ca^{2+}/4-AP aCSF consisted of (mM): 4-AP 0.1, NaCl 124, KCl 5.25, KH_2PO_4 1.25, $MgSO_4$ 1.5, $NaHCO_3$ 26, Dextrose 10 and $CaCl_2$ 0.2.

A Michigan shank was inserted into the unfolded hippocampus along the dendritic-soma axis to measure the extracellular potentials. Electrical field amplitudes were calculated as the space derivative of potentials measured by two channels on the shank, one at the depth of cell layer (200 μm from the stratum) and one in apical dendrites (the channel immediately above). The Michigan shank was combined through a

multi-channel workstation with data acquisition system by Alpha omega, Inc. (AlphaLab SNR).

2.2.5 Electrical field effect modeling

To test the hypothesis that endogenous electric field alone could induce neural activity propagation, the synaptic connections, gap junctions, and diffusion effects were eliminated in the network. Neural activity of cells in Row A was first initiated by experimentally determined extracellular potential. Ten *in-vitro* signals acquired from each of the channels located at cell layer, apical dendrites, and basal dendrites by Michigan Shank were averaged and inserted extracellularly at corresponding locations in each cell of Row A in the model (**Fig. 2.3 A**). However, the extracellular potential amplitude required to initiate action potentials in Row A cells was approximately ten times larger than physiological amplitude. This is because physiological signals were acquired at its best 10 μm -30 μm away from its nearest cells due to the damage caused by the electrode insertion, while in the model, signals were inserted right outside of the membrane. As extracellular potential decays at a rate inversely proportional to the distance away from a point source, the potential amplitudes in the model were expected to be larger than what were seen physiologically.

The electric field effect was simulated using the quasi-static formulation of the Maxwell equations assuming homogenous volume conductors [27]. According to Ohm's Law for conductors in Maxwell's Equations, the potential φ at the point P at a distance r relatively to the reference electrode in a medium of conductivity σ is

$$\varphi = \frac{I}{4\pi\sigma r} \quad \textbf{(5)}$$

In the model, assuming the extracellular medium is homogeneous and linear, using superposition, **Eq. (5)** can be generalized to j monopolar electrodes from a total of i cells from the previous row(s) with a current $I_{i,j\to n}$ located at a distance $r_{i,j\to n}$ from the target node n for each target node n of the target cell. The extracellular potential inserted at target node n is given by

$$\boldsymbol{V_{ex,n} = \frac{SF}{4\pi\sigma}\sum_{cell\ i}\sum_{j}^{35}\frac{I_{i,j\to n}}{r_{i,j\to n}}} \quad \textbf{(6)}$$

where $\boldsymbol{V_{ex,n}}$ is the extracellular potential inserted at target node **n** in the target cell, $\boldsymbol{I_{i,j\to n}}$ is the membrane current (assuming current going out of the cell to be positive direction) at a node **j** of cell **i** located $\boldsymbol{r_{i,j\to n}}$ distance from target node **n**,with a total **j=35** nodes in each cell **(Fig. 2.3 B)**; **σ** is the extracellular conductivity (typically the extracellular resistivity is 250-380 Ωcm [28], [29]; 300Ωcm was used in the model); **SF** is the stacking factor. The electric field effect could only propagate in the transverse direction to simplify the model; Row B cells were affected by Row A cells, and Row C cells were affected by both Row A and Row B cells with the electric field effect.

2.2.6 Propagation speed and resulting network electric field measurement

The propagation speed was measured based on the intracellular recording of each row's middle cell, where the first spike's peaking time from each cell was recorded and the delay from Row A to Row B and from Row B to Row C were calculated. The propagation speed was derived by taking the travelling distance divided by delay time. To measure the resulting electrical field due to the network firing activity and compare it to the experimentally recorded waveforms, we placed three virtual electrodes (v1, v2, and v3) outside of the network (**Fig. 2.4 A**) vertically to test the network field amplitude,

similar to the placement of Michigan Shank electrodes in the *in-vitro* slice. The middle electrode was placed 30 μm away from the Row C middle cell to account for approximately three rows of dead cells around the electrode. Each row's resulting extracellular voltage toward v1, v2, and v3 were calculated, and the summed field from all three row layers gives the value at each of the electrode position. The extracellular field was calculated by finding the average of the spatial difference of v1 and v2 and the spatial difference of v1 and v3 (Eq. 7).

$$E_{network} = \frac{\frac{V_2 - V_1}{d1} + \frac{V_3 - V_1}{d2}}{2} \quad \textbf{(7)}$$

An extracellular potential widening algorithm ("shifting algorithm") was applied for each cell's extracellular with a value of 20 to provide the most consistent spike width with experimental results (**Fig. 2.4 B**).

2.3 RESULTS

2.3.1 Electrical field effect alone can sustain neural activity propagation *in-silico*

During 4-AP/ low Ca^{2+} induced epileptiform activity in the CA1 region of unfolded hippocampus, extracellular recordings in cell layer (V_a) and apical dendrites (V_b) showed trains of bursting events (**Fig. 2.5 A**). Electrical field amplitude near the cell layer was estimated by taking the spatial derivatives of two voltage measurements. Among 65 spikes in five unfolded hippocampus tissues, field spiking amplitude was between 1.60-7.13mV/mm with a mean value of 3.5 ± 1.0mV/mm, where most of the distribution fell between 2.5-5mV/mm; the averaged mid-amplitude spike width was 8.57 ±1.66 ms (**Fig. 2.5 A**). The simulation results provided very similar spiking characteristics and amplitudes in all row layers of the network. With a representative SF value of 20 and d_{c-c} value of 2.94 μm, the extracellular field amplitudes were 0.99mV/mm, 1.14mV/mm, and 2.45mV/mm for Row A, B, and C layers respectively(**Fig. 2.4 A, Eq. 7**); the network field amplitude (summation of all three layers) was 4.58mV/mm. As Row A was the furthest and Row C was the closest to the three virtual field recording electrodes, Row A and Row C exhibited the lowest and highest field amplitudes, respectively. In the simulation, the number of spikes in an event was 10, while in experimental 4-AP/ low [Ca^{2+}] environment, intra-burst spikes vary from 1(singlet) to 8 across different CA1 pyramidal cells with a mean around 3 to 4 spikes [6], [30], [31]. This is because our model had a high-end value of g_{Na} in the physiological range, while Shuai et al.(2003) pointed out that there is almost a linear relationship between the spiking number and the increase of g_{Na}[19]. It should be noted however, that

most of the studies on neuronal activity propagation studies only focused on the first spike in every event; thus, it was much more crucial to mimic the characteristic of the first spike than the rest of the event in the model.

Over a range of SF values between 10 and 30, field amplitude increases as SF increases and was approximately 3-6mV/mm when SF is within the physiological range, which matched experimental data as well as previously reported weak field amplitude in hippocampal slices (below 5mV/mm, [32], [33]) and in the cortex (4.52mV/mm, [17]) (**Fig. 2.5 B**). From Row A to Row B and Row B to Row C, the activity of the first spikes was clearly propagating (**Fig. 2.5 B)**, suggesting that electrical field effect solely is responsible for neuronal activity propagation in the CA1 hippocampal network.

2.3.2 Neuronal propagation induced by electrical field effect travels with a speed of approximately 0.1m/s *in-silico* and *in-vitro*

Using the control parameters given in Table 1 and 2, the model reproduced the essential characteristics of the bursting activity seen in CA1 pyramidal cells. The resting potential, first spike amplitude, and first spike 50%-amplitude width were -61.5mV, 93.9mV, and 6.5ms, respectively, all falling into the experimentally measured ranges from CA1 pyramidal cell *in-vitro* studies (resting potential: -75mV~ -52mV; first spike amplitude: 70mV~ 103.2mV; and first spike mid-amplitude: approximately 1~8ms) [19], [30], [31], [34]). To understand the action potential threshold of the modeled cell, a 10ms intracellular current stimulus was injected, and an action potential fired at 12.09mV above the resting potential when the stimulus was at 0.132nA, matching the *in-vivo* measured threshold values (11.2mV~16.8mV above the resting potential) (**Fig. 2.6 A)**.

The transverse propagation speed across the entire network was evaluated based on the action potential peaking time delays of each row's middle cell (namely, cell #5 of each row in **Fig. 2.2 A**). This is because the middle cells experience the strongest field effect compare to other cells in the row based on **Eq.6**. We recorded action potential waveforms and calculated the propagation speeds by taking distance travelled from Row A to Row C divided by the total action potential delay time (Δt1+Δt2). **Fig. 2.6 B** shows sample membrane potential signals with d_{c-c} of 2.94 μm and SF equaled to 20. With only electrical field effect in the network, neuronal activity propagated from Row A to Row C with a total traveling distance of 35.88 μm (three soma diameters plus two d_{c-c}) and a total time delay of 0.385ms, resulting a propagation speed of 0.093m/s . Within the physiological SF range, propagation speed increases as SF becomes bigger, as a more packed cellular network creates a bigger network field amplitude (**Fig. 2.5 B**) thus increasing the propagation speed. The mean speed was 0.12±0.097m/s (**Table 2.2)**.

2.3.3 Electrical field propagation also occurs in the normal channel dynamics

To determine if the effect described above is robust, we tested the field effect in a CA1 pyramidal network using normal channel kinetic equations with an established model by Wimmer et al. [35]. Each cell contained 15 different distributed Ca^{2+} and voltage-dependent conductances and produces an intracellular signal that captures the physiological action potential characteristics upon initial stimulation (**Fig. 2.7 A**). The number of compartments in each cell, the network layout, and neuronal activity initiation using Michigan Shank acquired recordings remained the same, and the speed and network field amplitude were tested with a mean d_{c-c} = 2μm and variance of 0.1μm for

each value of SF (n=10 for each of SF=10, 15, 20, 25, and 30) in the same way described previously. Results showed that the mean propagation speed upon neuronal activity initiation was 0.11±0.03 m/s (**Fig. 2.7 B and D**) and the field amplitude ranged from 2.33~3.06mV/mm (**Fig. 2.7 C and E**) within physiological SF range, both match the speed and field amplitude seen *in-vitro* and *in-vivo*. This predicts that electrical field effect alone can not only produce neuronal activity propagation in pathological epileptiform-inducing environments, but also in networks with normal channels kinetics.

2.3.4 Electrical field effect explains the inverse relationship between extracellular osmolarity and propagation speed

To test the model prediction that the speed of propagation decreases with increasing distance between the neurons, we performed osmolarity experiments *in-vitro* and found a similar relationship between the change in extracellular space volume and the resulting neuronal activity propagation speed. The experiments were carried out in longitudinal mice slices in 4-AP solutions as propagation is usually the strongest in that direction [9]. By decreasing the osmolarity (cell swells and d_{c-c} decreases) of 4-AP aCSF by 270-275 mOsm, time delay between signals measured from two glass pipettes located along the CA3 layer decreased from 13.98 ± 4.08 ms (n=86 spike-pair from 3 slices) to 9.43 ± 4.97 ms (n=138 spike-pair from 3 slices in low osmolarity over 10 mins after dilution). With an estimated distance between the two glass pipettes equals to 0.6mm, a 48.3% increase in speed was seen. On the other hand, by increasing the osmolarity (cell shrinks and d_{c-c} increases) of 4-AP aCSF by ~30 mOsm after adding mannitol, time delay increased from 5.95 ±1.12ms (26 spike-pair from 1 slice) to 9.76 ±

1.78 ms (50 spike-pair from 1 slice in high osmolarity over 40 mins after concentrating the solution), corresponds to a 40.0% decrease in speed (**Fig. 2.8 A**). The same relationship was shown in the simulation. Taking d_{c-c} = 3μm as the control group, the propagation speed increased by 130% when d_{c-c} decreased to ~2μm, and decreased by 50% when mean d_{c-c} increased to ~4μm (**Fig. 2.8 B**). Furthermore, as SF goes up (higher cellular volume density and similar as lower osmolarity), propagation speed goes up (**Fig. 2.6 C**), which provides additional matching trend as osmolarity changes.

These results confirm the predictions of the model regarding the effect of cell-to-cell distance on the speed of propagation. The experimental results are also consistent with the effect of osmolarity on speed of propagation that was previously reported [36] and showed that the strength of electrical field effect plays a significant role in determining the neuronal activity propagation speed. For instance, a tightly packed network (low osmolarity or smaller d_{c-c}) increases the electrical impedance and field sensitivity between cells [15], [18], which in turn strengthens the amplitude of electrical field during neuronal activity propagation. It has also been shown previously that externally applied field can linearly affect changes in action potential timing; namely, the stronger the field strength, the sooner cells fire [32]. Interestingly, in our simulation, we found a similar relationship between the field amplitude and the propagation time delay for every cell-to-cell distance group (**Fig. 2.9**). This effect can explain why extracellular osmolarity has an inverse relationship with propagation speed and emphasize the important effect of endogenous network field strength on the neuronal activity propagation speed.

2.4 DISCUSSION

The observation that neural activity can propagate at a speed of approximately 0.1m/s in either physiological (theta wave) or pathological (epileptiform) conditions and in the presence or absence of chemical/electrical synapses suggest the a common novel mechanism for neural communication is involved. Previous studies related to such type of propagation eliminated the possibility for chemical synapses, gap junctions, axonal conductions, and ionic diffusion [2], [3], [9], [10], [11], [13], [14], and the only remaining explanation for the governing mechanism is electrical field effect. This electrical effect was thought to be too small to give rise to an action potential [16], [37], and to our knowledge, most of the previous studies involve externally applied field signal to show how a field can modify neuronal activity [16], [32], [37], [38]. Francis et al. demonstrated that a neuronal network is much more sensitive to field modulation than the average single neuron threshold, and that the highly structured and dense cellular packing in hippocampus makes the region of the brain highly sensitive to field effects [15]. The propagation of neural activity at 0.1m/s was recently observed in the hippocampus and attributed to field effects by default [9] . This simulation not only allowed us to directly examine if the field effect can solely govern the propagation of neuronal activity within a hippocampal CA1 pyramidal network connected with no other means (such as synapses or gap junctions), but also provides further information on how endogenous field strength (amplitude) relate to extracellular osmolarity and propagation speed both in simulation and experiments. Together, this study confirms that electric field effect with strength within the physiological range can be high enough to generate propagation of neural activity.

The cellular network in the simulation consists of 30 hippocampal CA1 pyramidal cell locations (10 cells/row×3 rows, **Fig. 2.2**), where cell-to-cell distances was between ~2 to ~4 μm [16], [20]. An arbitrary stacking factor (SF) was used to represent the physical stacking around each cell location, and the value of SF was derived from the physiological volume density in hippocampal CA1 region (physiological SF range = 15~28 based on volume density reported from [20], [23]). The model was validated as the field amplitude and field 50%-amplitude width produced in the simulation matched exactly *in-vitro* recordings of unfolded hippocampus through Michigan Shank (**Fig. 2.5**) and those known to generate electrical field effects in hippocampal slices (~5mV/mm) [32], [33] and in cortex (up to 4.52mV/mm) [17]. At the same time, the model successfully reproduced physiological intracellular spike characteristics both in a 4-AP/ Ca^{2+}-free (**Fig. 2.6 A**) and in normal aCSF environment (**Fig. 2.7 A**)

Upon initial extracellular stimulation through Michigan Shank acquired signals, transverse propagation of the activity was observed both with 4-AP/ Ca^{2+}-free (**Fig. 2.6 B** and normal channel kinetics in the simulation (**Fig. 2.7 B**). The average speed with cell-to-cell distances (d_{c-c}) equals to ~2 to ~4 μm was around 0.12 m/s for 4-AP/ Ca^{2+}-free conditions (**Table 2.2 and Fig. 2.6 C**) and 0.11m/s for normal channel kinetics conditions (**Fig. 2.7 B and D**), matching the common 0.1m/s speed reported in epileptiform propagation [2], [3],[4], [5], low Ca^{2+} field bursting [6], and theta oscillations both in-vitro [7] and in-vivo [1]. Since the cells in the simulated network were connected only through field effect, these results indicate that field effect itself can be solely responsible for neuronal activity propagation with a speed of 0.1m/s in a cellular network independently of channel kinetics.

The electrical field effect can also explain the effect of tissue osmolarity on neuronal propagation speed. In the present study, 4-AP induced epileptiform activity travelled faster when extracellular osmolarity was lowered (cells swelling), and vice versa (**Fig. 2.8 A**), matching the relationship between osmolarity and propagation speed in low Mg^{2+} -induced seizure activity in hippocampal CA1 region [32]. These experimental results confirmed the prediction from the simulations that a lower d_{c-c} (smaller extracellular space) produces a faster propagation speed (**Fig. 2.8 B**) because as the distance between cells decreased, the network field amplitude increased (**Fig. 2.5 B Right**). Radmen et al. suggested that there is a linear relationship between applied field amplitude and changes in action potential timing: the stronger the field strength, the sooner cells fire [32]. Interestingly, we found that the network field amplitude and propagation delay has a similar inverse linear relationship (**Fig. 2.9**); thus, the speed increases as field amplitude increases. Thus, the hypothesis that propagation of neural activity can be carried out solely by electric fields is consistent with experimental data as well as computer simulation results.

Ionic Channels	Maximum Conductance Values
g_{Na}	$0.045\ S/cm^2$
g_{NaP}	$0.0003\ S/cm^2$
g_{KDR}	$0.01\ S/cm^2$
g_{KA}	$0.007\ S/cm^2$
g_{m}	$0.059\ S/cm^2$
$g_{leak,soma}$	$0.001\ S/cm^2$
$g_{leak,dendrites}$	$2.922\times10^{-5} S/cm^2$

Table 2.1. Maximum conductance values used in the model

Mean d_{c-c}	Mean Speed (Within Physiological SF Range)
2 μm	0.23±0.096 m/s
3 μm	0.10±0.048 m/s
4 μm	0.05±0.020 m/s
~2 to ~4 μm	**0.12 ± 0.097 m/s**

Table 2.2. Mean propagation speeds for various cell-to-cell distances within the physiological SF range

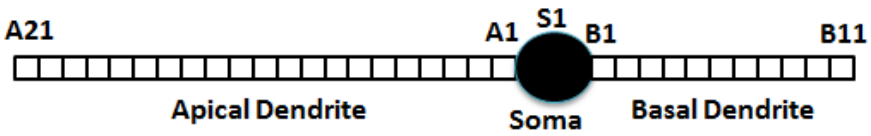

Figure 2.1. Structure of CA1 pyramidal cell model. There are 21 compartments in the apical dendrite (A1-A21), one compartment in the soma (S1), and 11 compartments in the basal dendrite (B1-B11)

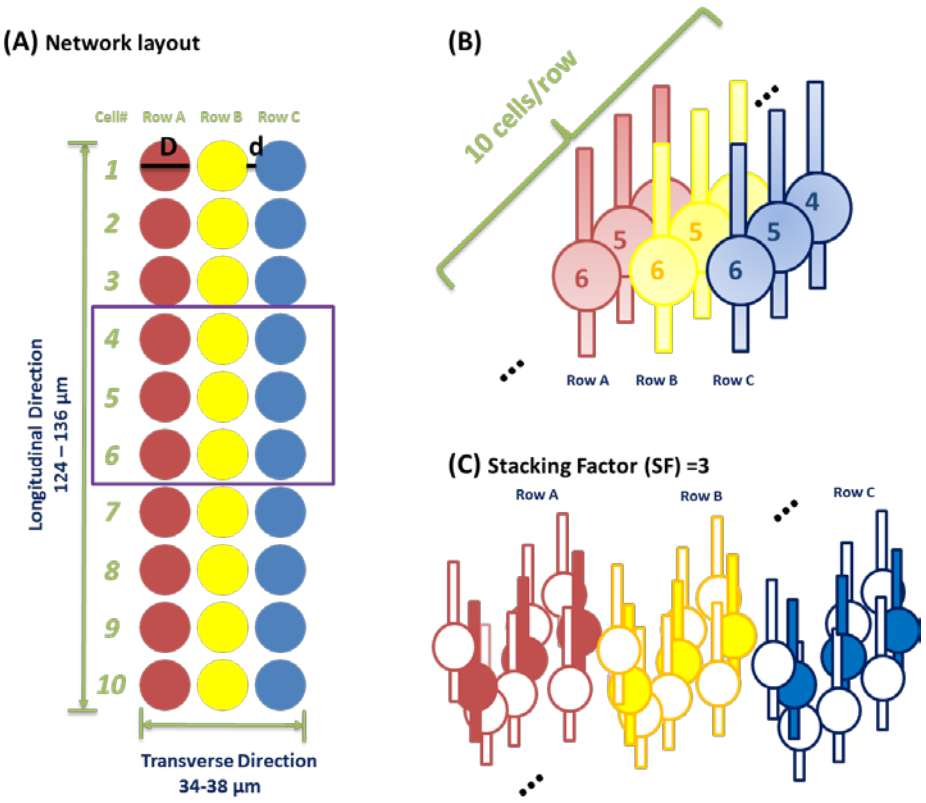

Figure 2.2. CA1 Pyramidal cellular network layout in the model. (A) Top view of the network (solid circles represent soma positions). The network contains three rows of cells with ten in each row, where the diameter of the soma is 10 µm and the soma edge-to-edge distance (d_{c-c}) range from 2 to 4 µm. Thus the dimension of the network is 34~38 µm ×124~136 µm. (B) 3-D view of the network. (C) Physical representation of the stacking factor (SF). In each row, solid-colored cells represent the actual modeled cells, while empty-colored cells represent the virtually stacked cells around the modeled cells. A stacking factor of 3 is shown in the figure, where each modeled cells were surrounded by two extra virtual cells at the spot and the amplitude of electrical field created by each modeled cells were multiplied by 3.

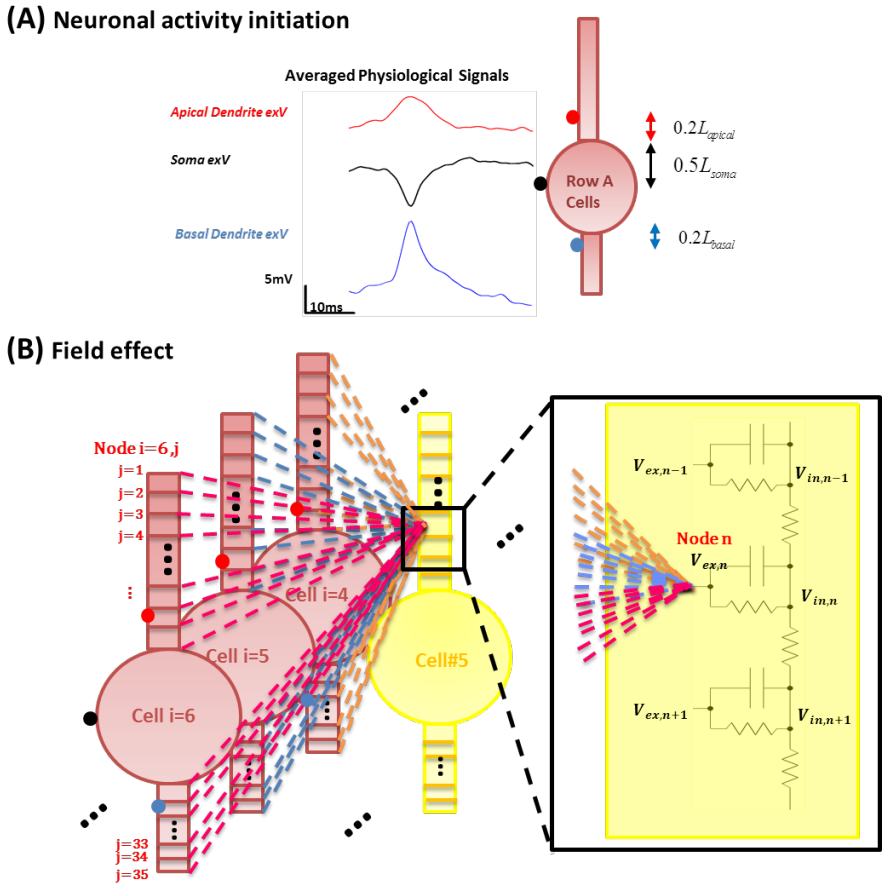

Figure 2.3. Initiation of neuronal activity and field effect computation within the network. (A) Initiation of the neuronal activity by extracellular stimulation for Row A cells using in-vitro acquired signal. Each of the three signals was ten times the average of 10 randomly selected trials from in-vitro acquired signals (i.e. cell layer, apical dendrites, basal dendrites). The signals were placed on the middle point of soma and dendrites close to the soma. (B) Network field effect acting on one extracellular node of a target cell using Eq.6. The field acting on node n of Row B Cell #5 was the superposition of all fields created from all Row A cells.

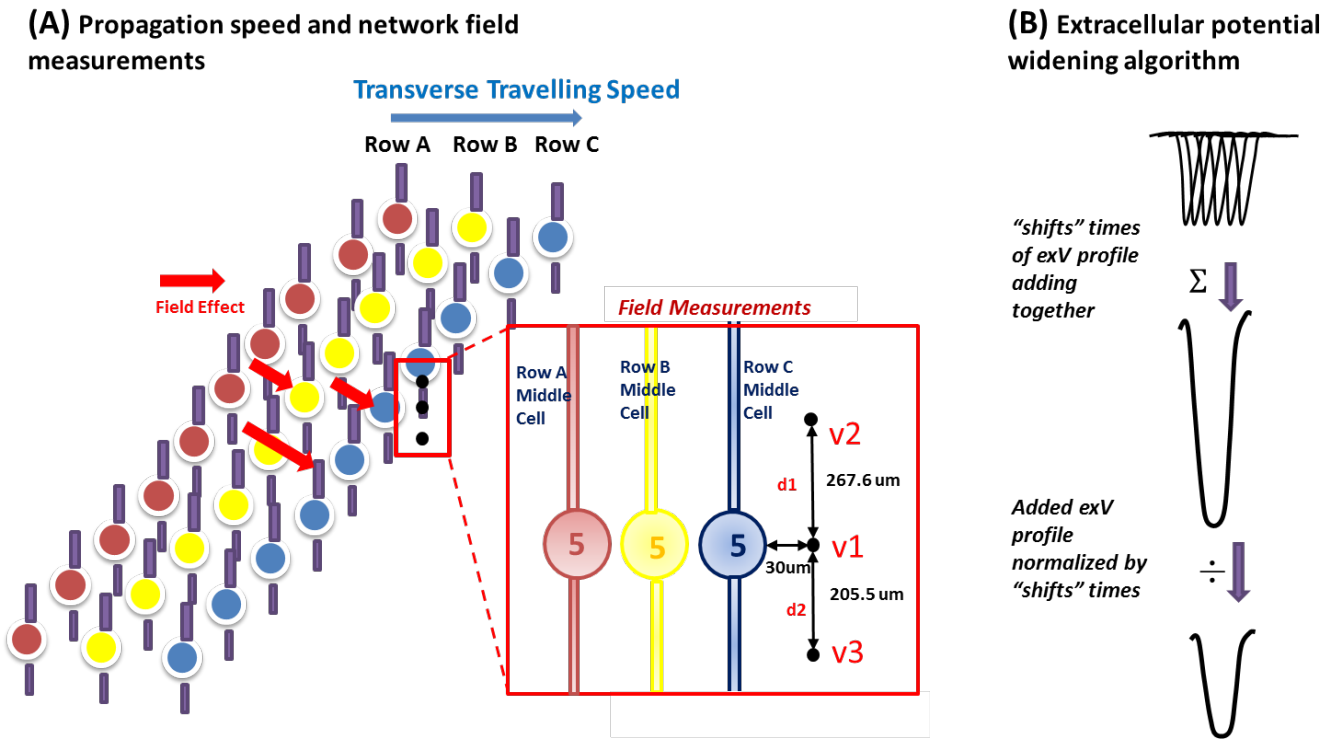

Figure 2.4 Propagation speed and field amplitude measurements in the model. (A) Transverse neuronal activity propagation and network extracellular field measurement. Row A affects Row B, and Row A and Row B affect Row C through electrical field effect. Three virtual electrodes were placed 30 μm away from the third row middle cell the extracellular voltages resulting from all of the cells in Row A, B, and C were measured at v1, v2, and v3. The field amplitude was calculated as the average of the spatial difference of v1 and v2 and the spatial difference of v1 and v3 (Eq. 7). (B) Extracellular potential widening algorithm. "Shifting algorithm" procedure. Each recorded extracellular voltage waveform was widened by "shifts" times, and the sum of the shifted copies (each shifted by one time step) are then normalized by "shifts" times to preserve the amplitude of the measured extracellular voltage signal. The model used 20 as the value of "shifts", and resulting width of processed signal matched the width of the extracellular voltage signal acquired through Michigan Shank (See Results for more information).

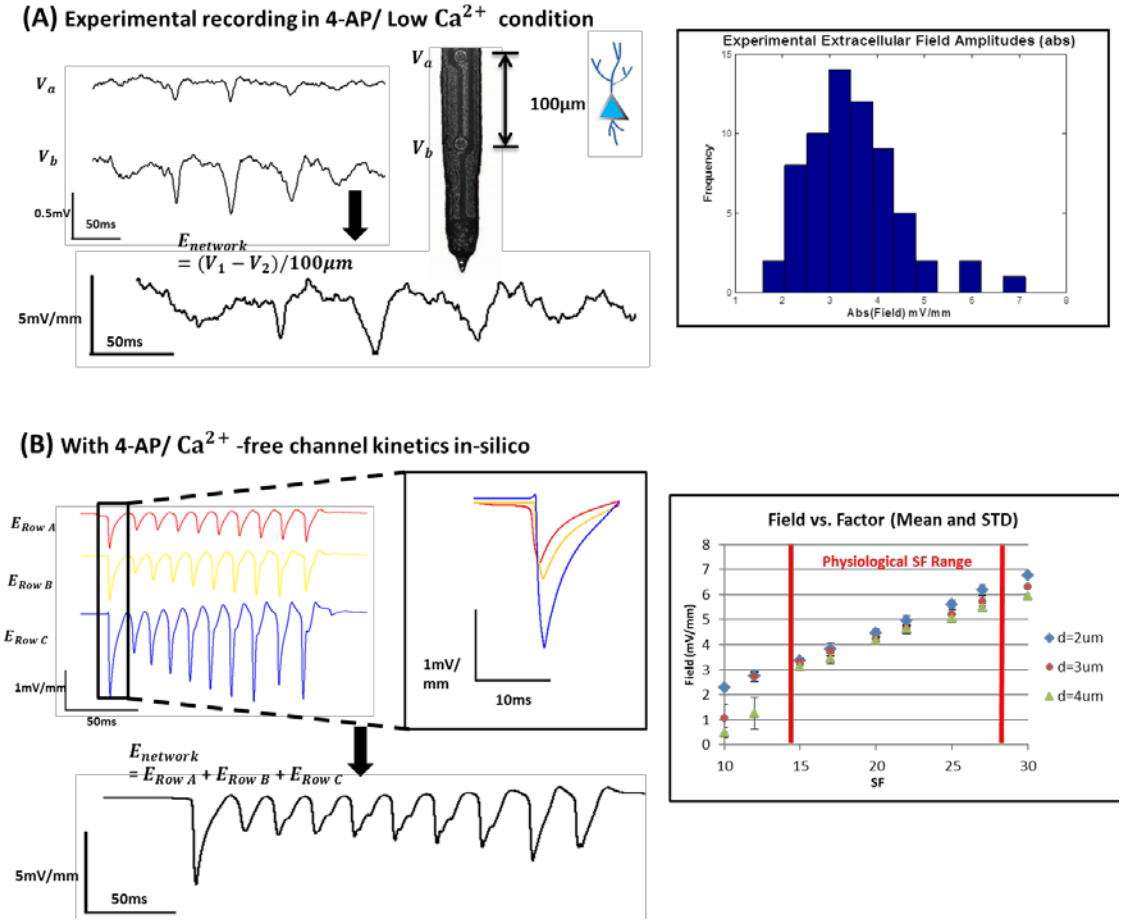

Figure 2.5. Simulation validation by *in-vitro* extracellular recordings. (A) Left: A typical cell layer (V_1) and apical dendrites (V_2) experimental recordings of extracellular potential and calculated network field by taking the space derivative of V_a and V_b. Right: A histogram of field amplitude among 65 spikes recorded from 5 unfolded hippocampus tissue suggests the field amplitude usually lays between 2.5-5mV/mm. (B) Left: Sample extracellular field recordings for Row A, B, and C layers with typical value of SF=20 and d_{c-c}=2.94 µm. The network field was calculated through the field signal summation of all three layers. Propagation of the activity was clearly seen in the first spike of every row layer. Right: Over physiological range of SF, network field amplitude ranged from 3-6mV/mm, where it increases as SF increases (tighter packing).

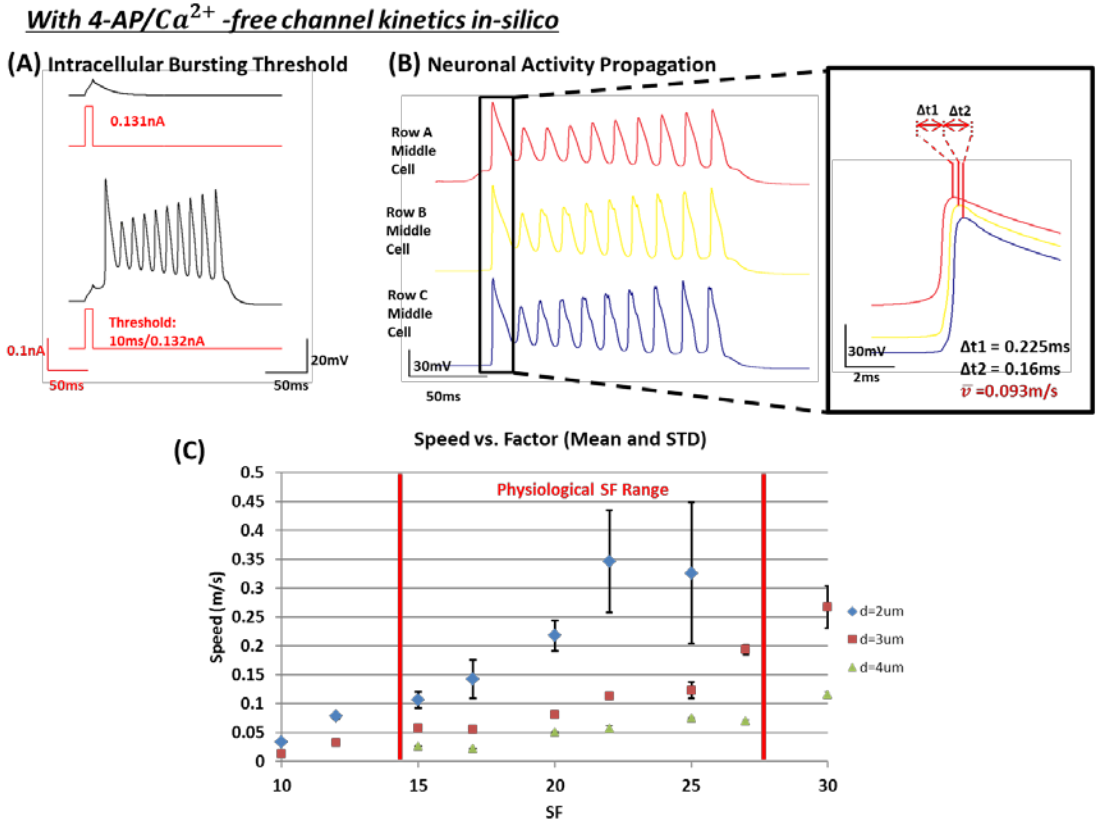

Figure 2.6. Transverse propagation speed as a function of field effect with 4-AP/Ca^{2+} free channel kinetics in simulation. (A) Intracellular activity fires action potential with an intracellular stimulus of 10ms/0.132nA, and the resulting waveform captures the essential physiological characteristics. (B) A typical set of intracellular waveforms of the middle cell in Row A, B, and C upon initial extracellular stimulation by Michigan Shank acquired signals. With SF=20 and d_{c-c}=2.94μm, delays of 0.225ms and 0.16ms were recorded between the first spike peaking time of Row A and Row B middle cells and Row B and Row C middle. The neuronal activity travelled through a total distance of 35.88 μm (three soma diameters plus two d_{c-c}), and with a total delay of 0.385ms, the propagation speed across the three rows was 0.093m/s. (C) Propagation speed at various SF (10~30) and d_{c-c} (2,3, or 4μm) with n=10 for each SF and d_{c-c}. Within physiological SF range (15-27 based on physiological volume density at hippocampal CA1 region; range limits marked with vertical lines), the average speed was 0.12±0.097m/s for d_{c-c}=2~4μm. Speed increases as SF goes up and d_{c-c} goes down.

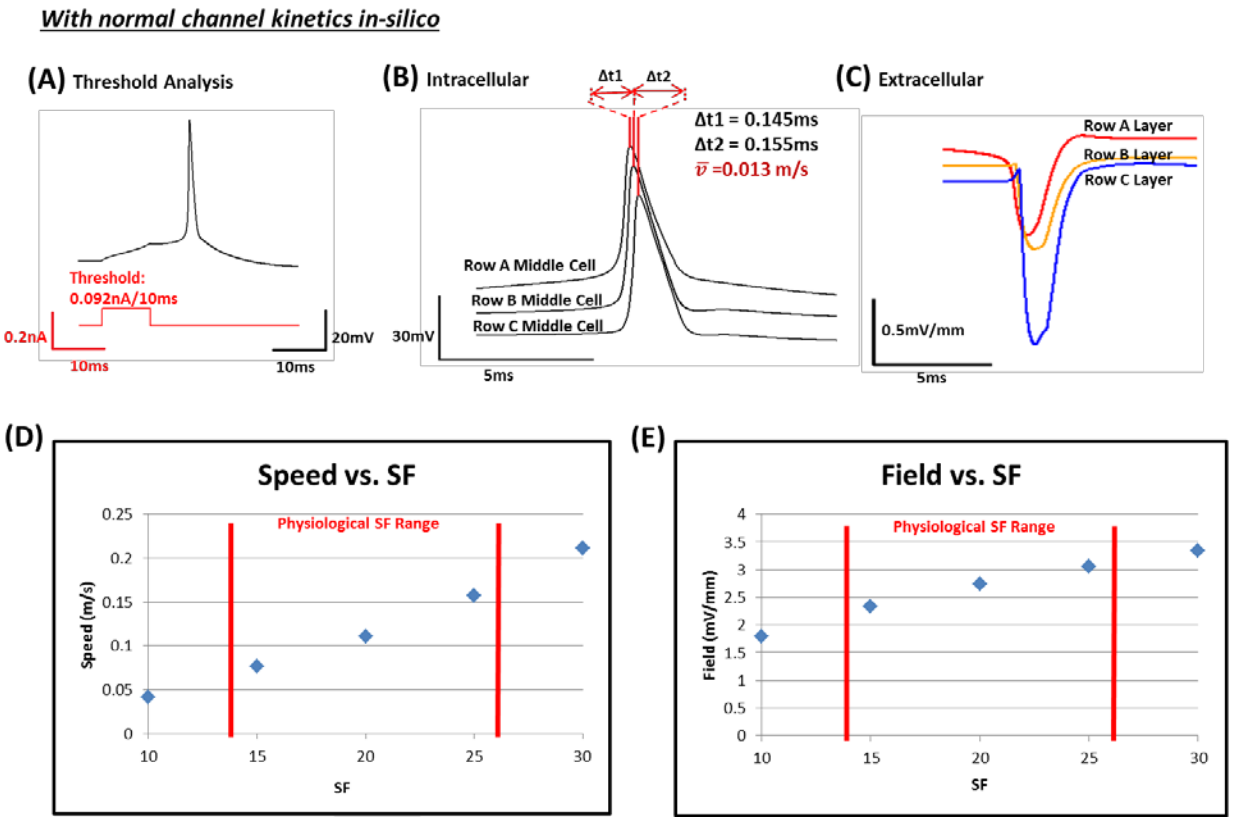

Figure 2.7. Resulted transverse propagation speed and field amplitude by field effect with normal channel kinetics in simulation. (A) With normal channel kinetics, modeled pyramidal cell fires at an intracellular stimulation threshold of 0.092nA/10ms, and the action potential exhibits essential physiological action potential characteristics. (B) A sample set of intracellular recording of Row A, Row B, and Row C middle cells with SF=20 and d_{c-c}=1.93µm. The total propagation delay was 0.3ms, and with a travelling distance of 33.86µm (three soma diameters plus two d_{c-c}), the speed was 0.013m/s. (C) A sample set of extracellular field recording with SF=20 and d_{c-c}=1.93µm. The field amplitude was 0.68 mV/mm, 0.72mV/mm, and 1.43mV/mm for Row A, Row B, and Row C layers, resulting a total network field amplitude of 2.83mV/mm. (D) Propagation speed at various SF with mean d_{c-c}=2µm (n=10 and variance=0.1µm for each SF). The speed goes up as SF increases, and within physiological SF range, the mean propagation speed is around 0.1m/s. (E) Network field amplitude at various SF with mean d_{c-c}=2µm (n=10 and variance=0.1µm for each SF). The field goes up as SF increases, and within physiological SF range, network field amplitude ranges from ~2-~3mV/mm, matching reported weak field amplitude seen *in-vitro*.

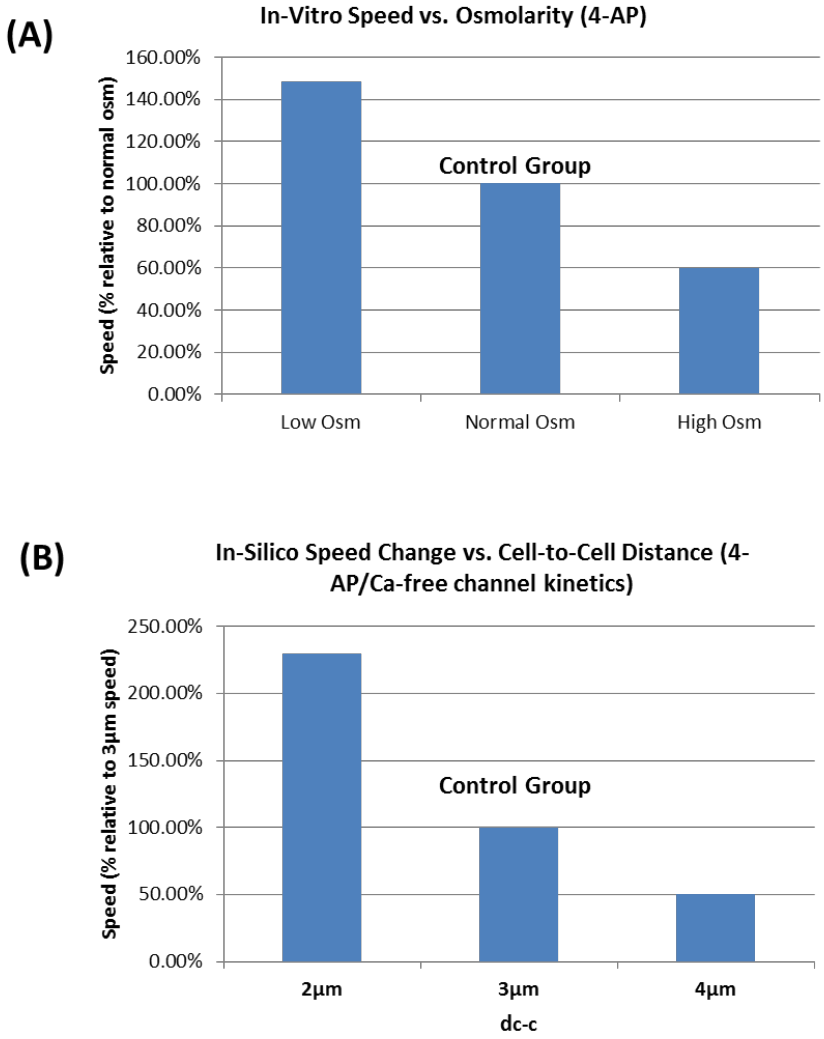

Figure 2.8. The inverse relationship between extracelluar osmolarity (or extracellular space) and propagation speed recorded *in-vitro* and *in-silico*. (A) Effect of osmolarity on speed of propagation in-vitro. Compared to epileptiform activity in normal osmolarity of the 4-AP solution, propagation speed increased at low osmolarity (cell swellings and decreased d_{c-c}) and decreased at high osmolarity (cell shrinking and increased d_{c-c}). (B) Effect of distance between cells (extracellular space) on the speed of propagation *in-silico*. Using d_{c-c}=3µm as control group, propagation speed increased when d_{c-c} decreased, and decreased when d_{c-c} increased.

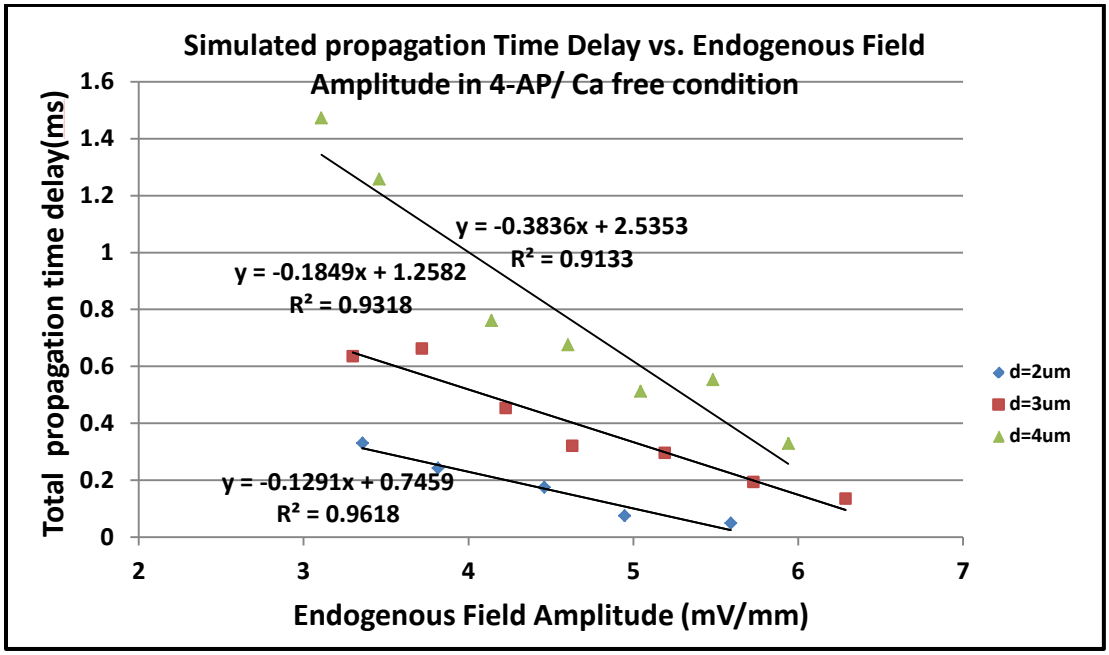

Figure 2.9. The linear relationship between simulated neuronal activity travelling delay time (from Row A to Row C) and endogenous network field amplitude. For each d_{c-c} group, the time delay decreases linearly as field amplitude increases.

2.5 References

[1] E. V. Lubenov and A. G. Siapas, “Hippocampal theta oscillations are travelling waves,” *Nature*, vol. 459, no. 7246, pp. 534–539, May 2009.

[2] A. B. Kibler and D. M. Durand, “Orthogonal wave propagation of epileptiform activity in the planar mouse hippocampus in vitro,” *Epilepsia*, vol. 52, no. 9, pp. 1590–1600, Sep. 2011.

[3] R. Miles, R. D. Traub, and R. K. Wong, “Spread of synchronous firing in longitudinal slices from the CA3 region of the hippocampus,” *J. Neurophysiol.*, vol. 60, no. 4, pp. 1481–1496, Oct. 1988.

[4] J.-S. Liu, J.-B. Li, X.-W. Gong, H.-Q. Gong, P.-M. Zhang, P.-J. Liang, and Q.-C. Lu, “Spatiotemporal dynamics of high-K+-induced epileptiform discharges in hippocampal slice and the effects of valproate,” *Neurosci. Bull.*, vol. 29, no. 1, pp. 28–36, Feb. 2013.

[5] P. P. Quilichini, D. Diabira, C. Chiron, Y. Ben-Ari, and H. Gozlan, “Persistent epileptiform activity induced by low Mg2+ in intact immature brain structures,” *Eur. J. Neurosci.*, vol. 16, no. 5, pp. 850–860, Sep. 2002.

[6] H. L. Haas and J. G. Jefferys, “Low-calcium field burst discharges of CA1 pyramidal neurones in rat hippocampal slices,” *J. Physiol.*, vol. 354, pp. 185–201, Sep. 1984.

[7] N. L. M. Cappaert, F. H. Lopes da Silva, and W. J. Wadman, “Spatio-temporal dynamics of theta oscillations in hippocampal-entorhinal slices,” *Hippocampus*, vol. 19, no. 11, pp. 1065–1077, Nov. 2009.

[8] M. Bikson, R. S. Ghai, S. C. Baraban, and D. M. Durand, “Modulation of burst frequency, duration, and amplitude in the zero-Ca(2+) model of epileptiform activity,” *J. Neurophysiol.*, vol. 82, no. 5, pp. 2262–2270, Nov. 1999.

[9] M. Zhang, T. P. Ladas, C. Qiu, R. S. Shivacharan, L. E. Gonzalez-Reyes, and D. M. Durand, “Propagation of epileptiform activity can be independent of synaptic transmission, gap junctions, or diffusion and is consistent with electrical field transmission,” *J. Neurosci. Off. J. Soc. Neurosci.*, vol. 34, no. 4, pp. 1409–1419, Jan. 2014.

[10] J. P. Meeks and S. Mennerick, “Action potential initiation and propagation in CA3 pyramidal axons,” *J. Neurophysiol.*, vol. 97, no. 5, pp. 3460–3472, May 2007.

[11] A. L. Jensen, “Control of Axonal Conduction of High Frequency Stimulation,” Case Western Reserve University, 2008.

[12] A. B. Kibler, B. G. Jamieson, and D. M. Durand, “A high aspect ratio microelectrode array for mapping neural activity in vitro,” *J. Neurosci. Methods*, vol. 204, no. 2, pp. 296–305, Mar. 2012.

[13] J. Lian, M. Bikson, J. Shuai, and D. M. Durand, “Propagation of non-synaptic epileptiform activity across a lesion in rat hippocampal slices,” *J. Physiol.*, vol. 537, no. Pt 1, pp. 191–199, Nov. 2001.

[14] F. Weissinger, K. Buchheim, H. Siegmund, U. Heinemann, and H. Meierkord, “Optical imaging reveals characteristic seizure onsets, spread patterns, and propagation velocities in hippocampal-entorhinal cortex slices of juvenile rats,” *Neurobiol. Dis.*, vol. 7, no. 4, pp. 286–298, Aug. 2000.

[15] J. T. Francis, B. J. Gluckman, and S. J. Schiff, “Sensitivity of neurons to weak electric fields,” *J. Neurosci. Off. J. Soc. Neurosci.*, vol. 23, no. 19, pp. 7255–7261, Aug. 2003.

[16] C. A. Anastassiou, R. Perin, H. Markram, and C. Koch, “Ephaptic coupling of cortical neurons,” *Nat. Neurosci.*, vol. 14, no. 2, pp. 217–223, Jan. 2011.

[17] F. Fröhlich and D. A. McCormick, “Endogenous Electric Fields May Guide Neocortical Network Activity,” *Neuron*, vol. 67, no. 1, pp. 129–143, Jul. 2010.

[18] E. J. Vigmond, J. L. Perez Velazquez, T. A. Valiante, B. L. Bardakjian, and P. L. Carlen, “Mechanisms of electrical coupling between pyramidal cells,” *J. Neurophysiol.*, vol. 78, no. 6, pp. 3107–3116, Dec. 1997.

[19] J. Shuai, M. Bikson, P. J. Hahn, J. Lian, and D. M. Durand, “Ionic mechanisms underlying spontaneous CA1 neuronal firing in Ca2+-free solution,” *Biophys. J.*, vol. 84, no. 3, pp. 2099–2111, Mar. 2003.

[20] M. A. Kurt, M. I. Kafa, M. Dierssen, and D. C. Davies, “Deficits of neuronal density in CA1 and synaptic density in the dentate gyrus, CA3 and CA1, in a mouse model of Down syndrome,” *Brain Res.*, vol. 1022, no. 1–2, pp. 101–109, Oct. 2004.

[21] E. N. Warman, D. M. Durand, and G. L. Yuen, “Reconstruction of hippocampal CA1 pyramidal cell electrophysiology by computer simulation,” *J. Neurophysiol.*, vol. 71, no. 6, pp. 2033–2045, Jun. 1994.

[22] A. L. Hodgkin and A. F. Huxley, “A quantitative description of membrane current and its application to conduction and excitation in nerve,” *J. Physiol.*, vol. 117, no. 4, pp. 500–544, Aug. 1952.

[23] S. Jinno and T. Kosaka, “Stereological estimation of numerical densities of glutamatergic principal neurons in the mouse hippocampus,” *Hippocampus*, vol. 20, no. 7, pp. 829–840, Jul. 2010.

[24] P. Perreault and M. Avoli, “Effects of low concentrations of 4-aminopyridine on CA1 pyramidal cells of the hippocampus,” *J. Neurophysiol.*, vol. 61, no. 5, pp. 953–970, May 1989.

[25] P. Perreault and M. Avoli, “4-aminopyridine-induced epileptiform activity and a GABA-mediated long-lasting depolarization in the rat hippocampus,” *J. Neurosci. Off. J. Soc. Neurosci.*, vol. 12, no. 1, pp. 104–115, Jan. 1992.

[26] L. E. Schechter, “The potassium channel blockers 4-aminopyridine and tetraethylammonium increase the spontaneous basal release of [3H]5-hydroxytryptamine in rat hippocampal slices,” *J. Pharmacol. Exp. Ther.*, vol. 282, no. 1, pp. 262–270, Jul. 1997.

[27] B. He, “Electrical stimulation of the neuromuscular system,” in *Neural Engineering*, 2005th ed., vol. 3, Springer, 2005, p. 503.

[28] C. Gold, D. A. Henze, and C. Koch, “Using extracellular action potential recordings to constrain compartmental models,” *J. Comput. Neurosci.*, vol. 23, no. 1, pp. 39–58, Aug. 2007.

[29] N. K. Logothetis, C. Kayser, and A. Oeltermann, “In vivo measurement of cortical impedance spectrum in monkeys: implications for signal propagation,” *Neuron*, vol. 55, no. 5, pp. 809–823, Sep. 2007.

[30] D. Golomb, C. Yue, and Y. Yaari, “Contribution of persistent Na+ current and M-type K+ current to somatic bursting in CA1 pyramidal cells: combined experimental and modeling study,” *J. Neurophysiol.*, vol. 96, no. 4, pp. 1912–1926, Oct. 2006.

[31] H. Su, G. Alroy, E. D. Kirson, and Y. Yaari, “Extracellular calcium modulates persistent sodium current-dependent burst-firing in hippocampal pyramidal neurons,” *J. Neurosci. Off. J. Soc. Neurosci.*, vol. 21, no. 12, pp. 4173–4182, Jun. 2001.

[32] T. Radman, Y. Su, J. H. An, L. C. Parra, and M. Bikson, “Spike timing amplifies the effect of electric fields on neurons: implications for endogenous field effects,” *J. Neurosci. Off. J. Soc. Neurosci.*, vol. 27, no. 11, pp. 3030–3036, Mar. 2007.

[33] R. S. Ghai, M. Bikson, and D. M. Durand, “Effects of applied electric fields on low-calcium epileptiform activity in the CA1 region of rat hippocampal slices,” *J. Neurophysiol.*, vol. 84, no. 1, pp. 274–280, Jul. 2000.

[34] J. Deuchars and A. M. Thomson, “CA1 pyramid-pyramid connections in rat hippocampus in vitro: dual intracellular recordings with biocytin filling,” *Neuroscience*, vol. 74, no. 4, pp. 1009–1018, Oct. 1996.

[35] V. C. Wimmer, C. A. Reid, S. Mitchell, K. L. Richards, B. B. Scaf, B. T. Leaw, E. L. Hill, M. Royeck, M.-T. Horstmann, B. A. Cromer, P. J. Davies, R. Xu, H. Lerche, S. F. Berkovic, H. Beck, and S. Petrou, “Axon initial segment dysfunction in a mouse

model of genetic epilepsy with febrile seizures plus," *J. Clin. Invest.*, vol. 120, no. 8, pp. 2661–2671, Aug. 2010.

[36] E. Shahar, M. Derchansky, and P. L. Carlen, "The role of altered tissue osmolality on the characteristics and propagation of seizure activity in the intact isolated mouse hippocampus," *Clin. Neurophysiol. Off. J. Int. Fed. Clin. Neurophysiol.*, vol. 120, no. 4, pp. 673–678, Apr. 2009.

[37] C. Y. Chan and C. Nicholson, "Modulation by applied electric fields of Purkinje and stellate cell activity in the isolated turtle cerebellum," *J. Physiol.*, vol. 371, pp. 89–114, Feb. 1986.

[38] C. A. Anastassiou, S. M. Montgomery, M. Barahona, G. Buzsáki, and C. Koch, "The effect of spatially inhomogeneous extracellular electric fields on neurons," *J. Neurosci. Off. J. Soc. Neurosci.*, vol. 30, no. 5, pp. 1925–1936, Feb. 2010.

CHAPTER 3

CONCLUSIONS

The primary objective of this study was to investigate whether electrical field effect alone can retain neuronal activity propagation in a cellular network and how the field amplitude modulates the propagation pattern and traveling speed. A computational model consisting of three rows of CA1 pyramidal cells connected with no other means but electrical field effect and the algorithm for field effect mathematical representation was developed (*Hypothesis I, Section 1.2*). This model could be repeatedly used as a testing platform for examining the role and significance of field effect for various types of neuronal activity propagation in any cellular network with corresponding channel kinetics.

Upon neuronal activity initiation in the first row, the speed and network field amplitude were measured. The results showed that with the field effect alone, a transverse propagation of neuronal activity was observed and the network field amplitude during propagation was around 2-5mV/mm in both normal conditions (normal channel kinetics) and pathological epileptiform condition (4-AP/Ca free channel kinetics), matching what the field amplitude recorded in hippocampus and cortex during a travelling event experimentally. Thus, the hypothesis that electrical field effect solely can drive neuronal activity propagation within a cellular network appeared to be true (*Hypothesis II, Section 1.2*). The mean speeds for such field-effect-induced propagation was 0.11 ± 0.03m/s in normal channel kinetics and 0.12 ± 0.097 m/s with pathological

kinetics, matching the common 0.1m/s speed recorded from epileptiform propagation and theta wave previously *in-vivo* and *in-vitro*. This showed that this field-effect-driven propagation exhibits a speed of approximately 0.1m/s regardless of whether it is under normal or pathological conditions, confirming the *Hypothesis III in Section 1.2*.

In addition, we found that endogenous field could positively modulate the propagation speed, namely, the higher the field amplitude, the faster the activity travels. As cellular packing becomes tighter in the simulated network, propagation speed also increased. Thus, the electrical field effect explains the inverse relationship between osmolarity and speed seen in experiments, proving that the *Hypothesis IV in Section 1.2* is true.

Understanding the electrical field effect could lead to a better understanding in seizure generation, seizure suppression, and theta wave generation. For instance, based on the findings of the significance of endogenous electric field in epileptiform propagation, it might be possible to control seizure activity by injecting a cancelling field locally to terminate the seizure travelling across different locations in the brain. In addition, as disruptions of theta oscillation produces behavioral impairment, manipulating the strength of field effect could allow us “tune” the oscillation pattern back to normal.

Future work on this topic should focus on directly proving the governing role of field effect in any propagation events with 0.1m/s *in-vitro* and *in-vivo*. One way of doing this could be injecting a cancelling field amplitude locally and monitor whether neuronal activity travelling terminates at the location. In addition, it is essential to generate a set of generalized requirements where field effect, although it appears to be weak in amplitude, plays a significant role in maintaining and modulating the neuronal activity travelling

pattern. This can be achieved by testing the physiological significance of the field effect under different parameter settings in the model and verify by the experimental data if it is experimentally testable. Finally, it is essential to explore the role of field effect in pathological condition management such as epilepsy suppression, where modulating the strength of field may allow us to modify epileptiform propagation pattern and control seizure.

Appendix

NEURON Script for the Simulation Model

A.1 4-AP/ Ca^{2+} Cell kinetics and structure

```
Script written by: Chen Qiu in 2012/10
Cell kinetics based on:
J. Shuai, M. Bikson, P. J. Hahn, J. Lian, and D. M. Durand, “Ionic
mechanisms underlying spontaneous CA1 neuronal firing in Ca2+-free
solution,” Biophys. J., vol. 84, no. 3, pp. 2099–2111, Mar. 2003

E. N. Warman, D. M. Durand, and G. L. Yuen, “Reconstruction of
hippocampal CA1 pyramidal cell electrophysiology by computer
simulation,” J. Neurophysiol., vol. 71, no. 6, pp. 2033–2045, Jun. 1994.


RmDend=34200 //Ohm.cm2
RmSoma= 680 //Ohm.cm2

Cm=1

RaAll=530 //Ohm.cm Axial or Cytoplasmic Resistance

Vrest = -65
dt = 0.0125

gna =  0.045//S/cm2
gkdr = 0.01 //S/cm2
gnap = 0.0003 //S/cm2
gka = 0.007 //S/cm2
gm = 0.003 //S/cm2
gl = 0.001 //S/cm2
gldend = 2.922e-5 //S/cm2


//Start creating the cell

nbasal=1
napical = 1
apicalseg = 21
basalseg = 11

Lapical = 735.3//um
Lbasal = 490.2 //um
Lsoma=10 //um
```

```
diamDend=5.2

create soma, basal[1], apical[1]

eqk=-80
eqna=65


soma {
pt3dclear()
    pt3dadd(-8.0,  0,  0.0,  4.273)
    pt3dadd(-7.31577,0,0, 5.566)
    pt3dadd(-6.25,  0,  0.0,  8.05716)
    pt3dadd(-5.23,  0,  0.0,  9.0)
    pt3dadd(-4,  0,  0.0,  9.4352)
    pt3dadd(-3.29923,  0,  0.0,  9.72981)
    pt3dadd(0,  0,  0.0,  10)
    pt3dadd(3.29923,  0,  0.0,  9.72981)
    pt3dadd(4,  0,  0.0,  9.4352)
    pt3dadd(5.23,  0,  0.0,  9.0)
    pt3dadd(6.25,  0,  0.0,  8.05716)
    pt3dadd(7.31577,0,0, 5.566)
    pt3dadd(8.0,  0,  0.0,  4.273)

insert na  gnabar_na=gna ena=eqna
insert kdr gkdrbar_kdr=gkdr ek=eqk
insert nap gnapbar_nap=gnap ena=eqna
insert ka gkabar_ka=gka ek=eqk
insert m gmbar_m=gm ek=eqk
insert leak glbar_leak=gl ecl=-60


//ar2_na3=0.8
insert pas e_pas=Vrest g_pas = 1/RmSoma
Ra=RaAll cm=Cm
nseg = 1
insert extracellular
}


for i=0, napical-1 apical[i]{
  pt3dclear()
  pt3dadd(4.45,0,0, diamDend)
  pt3dadd(4.45+Lapical,0,0,diamDend)

  nseg= apicalseg
  cm = Cm//uF/cm2
  //diam = 5.2 //um
  //L = Lapical //um
  Ra = RaAll //Ohm.cm
  insert pas
  g_pas = 1/RmDend // S/cm
  e_pas = Vrest //mV
  insert leak glbar_leak=gldend ecl=-58
  insert extracellular
```

```
}

for i=0, nbasal-1 basal[i]{
  pt3dclear()
  pt3dadd(-4.45,0,0, diamDend)
  pt3dadd(-4.45-Lbasal,0,0,diamDend)

  nseg= basalseg
  cm = Cm //uF/cm2
  //diam = 5.2 //um
 // L = Lbasal //um
  Ra = RaAll //Ohm.cm
  insert pas
  g_pas = 1/RmDend // S/cm
  e_pas = Vrest //mV
  insert leak glbar_leak=gldend ecl=-58
  insert extracellular
  }

//Connecting everything together
connect basal[0](0),soma(0)
connect apical[0](0), soma(1)
```

A.2 Normal cell kinetics and structure

```
Script written by Chen Qiu in 2013/11
Based on Wimmer et al. 2010 Complex CA1-neuron to study AP initiation
http://senselab.med.yale.edu/modeldb/ShowModel.asp?model=123927&file=\W
immer-et-al2009\Fig8a.hoc

RmDend=34200 //Ohm.cm2
RmSoma= 680 //Ohm.cm2

Cm=1

RaAll=530 //Ohm.cm Axial or Cytoplasmic Resistance

Vrest = -65
dt = 0.0125

gna =  0.045//S/cm2
gkdr = 0.01 //S/cm2
gnap = 0.0003 //S/cm2
gka = 0.007 //S/cm2
gm = 0.003 //S/cm2
gl = 0.001 //S/cm2
gldend = 2.922e-5 //S/cm2


//Start creating the cell
```

```
nbasal=1
napical = 1
apicalseg = 21
basalseg = 11

Lapical = 735.3//um
Lbasal = 490.2 //um
Lsoma=10 //um

diamDend=5.2

create soma, basal[1], apical[1]

eqk=-80
eqna=65


soma {
pt3dclear()
    pt3dadd(-8.0,  0,  0.0,  4.273)
    pt3dadd(-7.31577,0,0, 5.566)
    pt3dadd(-6.25,  0,  0.0,  8.05716)
    pt3dadd(-5.23,  0,  0.0,  9.0)
    pt3dadd(-4,  0,  0.0,  9.4352)
    pt3dadd(-3.29923,  0,  0.0,  9.72981)
    pt3dadd(0,  0,  0.0,  10)
    pt3dadd(3.29923,  0,  0.0,  9.72981)
    pt3dadd(4,  0,  0.0,  9.4352)
    pt3dadd(5.23,  0,  0.0,  9.0)
    pt3dadd(6.25,  0,  0.0,  8.05716)
    pt3dadd(7.31577,0,0, 5.566)
    pt3dadd(8.0,  0,  0.0,  4.273)

insert pas e_pas=Vrest g_pas = 1/RmSoma

//Ca current
 insert car
      PcaRbar_car = 4.4e-05
 insert cat
      PcaTbar_cat = 1e-05
 insert CAl
      PcalBar_CAl = 6.622e-05
 insert CAnpq
      PcanpqBar_CAnpq = 0.000154
 insert cadyn
      depth_cadyn = 1
      taur_cadyn = 1
      cainf_cadyn = 0.0001
 insert ca2dyn
      depth_ca2dyn = 1
      taur_ca2dyn = 1000
      ca2inf_ca2dyn = 0.0001

// K current
    insert KAHP //KAHP
```

```
      gAHPbar_KAHP = 0.0004

    insert KM //KM
      gMbar_KM = 0.0032
      timesTau_KM = 2
      plusTau_KM = 0

    insert kdrG //delayed rectifier KDR
      gbar_kdrG = 0.005

    insert kaG //KA
      gbar_kaG = 0.011

    insert kslow //fast K current (why called "slow"?)
      gbar_kslow = 0.012

    insert kleck //K leakage current
      gbar_kleck = 0.00004

    insert KCT //voltage and Ca dependent K current
      gCTbar_KCT = 0.02

    insert hd
      ghdbar_hd = 5e-06
      vhalfl_hd = -90

// Na current
    insert na3Mig //Transient Na Current
      sh_na3Mig = 0
      gbar_na3Mig = 0.1
      ar2_na3Mig = 1

    insert nap
      gbar_nap = 0.0003
      timestauh_nap = 50
      timestaum_nap = 1
      shifttaum_nap = 1
      shifttauh_nap = 1

    insert napIn
      gbar_napIn = 0.0008
      htau_napIn = 15




Ra=RaAll cm=Cm
nseg = 1
insert extracellular
}


for i=0, napical-1 apical[i]{
  pt3dclear()
```

```
  pt3dadd(4.45,0,0, diamDend)
  pt3dadd(4.45+Lapical,0,0,diamDend)

  nseg= apicalseg
  cm = Cm//uF/cm2
  //diam = 5.2 //um
  //L = Lapical //um
  Ra = RaAll //Ohm.cm
  insert pas
  g_pas = 1/RmDend // S/cm
  e_pas = Vrest //mV
insert leak
      glbar_leak=gldend ecl=-58

  insert extracellular
}

for i=0, nbasal-1 basal[i]{
  pt3dclear()
  pt3dadd(-4.45,0,0, diamDend)
  pt3dadd(-4.45-Lbasal,0,0,diamDend)

  nseg= basalseg
  cm = Cm //uF/cm2
  //diam = 5.2 //um
 // L = Lbasal //um
  Ra = RaAll //Ohm.cm
  insert pas
  g_pas = 1/RmDend // S/cm
  e_pas = Vrest //mV
  insert leak glbar_leak=gldend ecl=-58

  insert extracellular
  }

//Connecting everything together
connect basal[0](0),soma(0)
connect apical[0](0), soma(1)

//load_file("geometry.ses")

print "area= ",area(0.5)

stdrun=1
celsius=30
v_init=-75
cai0_ca_ion=5e-06
cao0_ca_ion=2
ca2i0_ca2_ion=5e-06
ca2o0_ca2_ion=2
```

A.3 Field effect calculation based on Eq. (6)

Algorithm developed and script written by Chen Qiu in 2012/8

```
rowBetween = SecondNeuronRow-FirstNeuronRow

objref factorFile
factorFile=new File()
factorFile.ropen("factor.txt")
factor = factorFile.scanvar()
printf("Our factor is %d\n", factor)


//Define extracellular resistivity and position of the electrode
x_soma=randomD*rowBetween//um
x_dend=randomD*rowBetween//um
//minimum distance between the position of the electrode and dendrite
//This is the distance between the edge of dendrites when the somas are
touching each other in an complete simulation case
rhoa=330//Ohm.cm


//Calculate the corresponding extracellular voltages at each position
objref Ve_apical2apical_n2[apicalSize], Ve_soma2apical_n2[somaSize],
Ve_basal2apical_n2[basalSize]
objref Ve_apical2soma_n2[apicalSize], Ve_soma2soma_n2[somaSize],
Ve_basal2soma_n2[basalSize]
objref Ve_apical2basal_n2[apicalSize], Ve_soma2basal_n2[somaSize],
Ve_basal2basal_n2[basalSize]

apicalSegL = Lapical/apicalseg
basalSegL = Lbasal/basalseg

//Calculate the corresponding extracellular voltages
objref Ve_n2_apical[apicalSize],
Ve_n2_soma[somaSize],Ve_n2_basal[basalSize] //These are for each point
in Neuron #3

for i1=0, (apicalSize-1){
Ve_n2_apical[i1]=new Vector(i_apical_n1[0][i1].size())
Ve_n2_apical[i1].fill(0)
}

for i2=0, (somaSize-1){
Ve_n2_soma[i2]=new Vector(i_soma_n1[0][i2].size())
Ve_n2_soma[i2].fill(0)
}

for i3=0, (basalSize-1){
Ve_n2_basal[i3]=new Vector(i_basal_n1[0][i3].size())
Ve_n2_basal[i3].fill(0)
}
```

```
//Recording the positions for (x,0)
objref apicalX, basalX
apicalX=new Vector(apicalSize)
basalX = new Vector(basalSize)

apical[0]{
aa=0
for(x,0){
apicalX.set(aa,x)
aa=aa+1
}
}

basal[0]{
bb=0
for (x,0){
basalX.set(bb,x)
bb=bb+1
}
}



for ii=1,n{
neuron2 = ii-1
if (ii>5) {neuron2=10-ii}


//-------------------------------------------------------------------------
-------
//This section is to calculate the extracellular voltages applied to
the apical dendrite of Neuron #2
//-------------------------------------------------------------------------
-------
j=0 k=0 a=0
for ia=0, (apicalSize-1){ //For each point on the apical dendrite of
Neuron #2
                // For each point on the apical dendrite of Neuron#2,
                 //the extracellular voltage should be the sum of all
of the extracellular voltages calculated
                 //from the apical dendrite, soma, and basal dendrite.

       //Calculate the corresponding extracellular voltages on apical
dendrites of Neuron#2
       //from apical dendrites of Neuron#1.

// *****

 //For every point on the apical dendrite of Neuron #1

for j=0, apicalSize-1{
r1 = sqrt(x_dend^2+(abs(n2-ii)*x_soma)^2+((abs(apicalX.x[ia]-
apicalX.x[j]))*Lapical)^2)
```

```
denominator1= 4* PI*r1/rhoa
Ve_apical2apical_n2[j] = new Vector(i_apical_n1[neuron2][j].size())
Ve_apical2apical_n2[j]=i_apical_n1[neuron2][j].c
Ve_apical2apical_n2[j].mul(factor*10^4/denominator1)

//Add the extracelluar voltage got from this specific point on Neuron#1
into the i point of Neuron #2
Ve_n2_apical[ia].add(Ve_apical2apical_n2[j])
}
// *****

//Calculate the corresponding extracellular voltages on apical
dendrites of Neuron#2
//from soma of Neuron#1.

for k=0, (somaSize-1){ //Soma is always lower than the apical dendrite,
so no worries about the vertical difference

r2 = sqrt(x_soma^2+(abs(n2-
ii)*x_soma)^2+(Lsoma/2+apicalX.x[ia]*Lapical)^2)
denominator2 = 4*PI*r2/rhoa
Ve_soma2apical_n2[k]=new Vector(i_soma_n1[neuron2][k].size())
Ve_soma2apical_n2[k]=i_soma_n1[neuron2][k].c
Ve_soma2apical_n2[k].mul(factor*10^4/denominator2)

Ve_n2_apical[ia].add(Ve_soma2apical_n2[k])
}
// *****

//Calculate the corresponding extracellular voltages on apical
dendrites of Neuron#2
//from distal dendrite of Neuron#1.
for a=0, (basalSize-1){
r3 = sqrt(x_dend^2+(abs(n2-
ii)*x_soma)^2+(basalX.x[a]*Lbasal+apicalX.x[ia]*Lapical+Lsoma)^2) //Seg
length on basal dendrite plus the entire length of soma plus the
distance of apical dendrite
denominator3 = 4*PI *r3/rhoa
Ve_basal2apical_n2[a]=new Vector(i_basal_n1[neuron2][a].size())
Ve_basal2apical_n2[a]=i_basal_n1[neuron2][a].c
Ve_basal2apical_n2[a].mul(factor*10^4/denominator3)

Ve_n2_apical[ia].add(Ve_basal2apical_n2[a])
}
}

//-----------------------------------------------------------------------
-------

//-----------------------------------------------------------------------
-------
//This section is to calculate the extracellular voltages applied to
the soma of Neuron #2
//-----------------------------------------------------------------------
-------
```

```
for ib=0, (somaSize-1){ //For each point on the soma of Neuron #2
j=0 k=0 a=0


                // For each point on the soma of Neuron#2,
                //the extracellular voltage should be the sum of all
of the extracellular voltages calculated
                //from the apical dendrite, soma, and basal dendrite
(superposition).

       //Calculate the corresponding extracellular voltages on soma of
Neuron#2
       //from apical dendrites of Neuron#1.
// *****

for j=0, (apicalSize-1){ //For every point from the apical dendrite of
Neuron #1
r1 = sqrt(x_dend^2+(abs(n2-
ii)*x_soma)^2+(apicalX.x[j]*Lapical+Lsoma/2)^2) //When the point on
Neuron#1 is positioned higher than the point on Neuron#2

denominator1= 4* PI*r1/rhoa
Ve_apical2soma_n2[j] = new Vector(i_apical_n1[neuron2][j].size())
Ve_apical2soma_n2[j]=i_apical_n1[neuron2][j].c
Ve_apical2soma_n2[j].mul(factor*10^4/denominator1)

//Add the extracelluar voltage got from this specific point on Neuron#1
into the i point of Neuron #2
Ve_n2_soma[ib].add(Ve_apical2soma_n2[j])
}
// *****

//Calculate the corresponding extracellular voltages on soma of
Neuron#2
//from soma of Neuron#1.

for k=0, (somaSize-1){  //For every point from the soma of Neuron #1
r2 = sqrt(x_soma^2+(abs(n2-ii)*x_soma)^2)
denominator2 = 4*PI*r2/rhoa
Ve_soma2soma_n2[k]=new Vector(i_soma_n1[neuron2][k].size())
Ve_soma2soma_n2[k]=i_soma_n1[neuron2][k].c
Ve_soma2soma_n2[k].mul(factor*10^4/denominator2)

Ve_n2_soma[ib].add(Ve_soma2soma_n2[k])
}
// *****



//Calculate the corresponding extracellular voltages on soma of
Neuron#2
//from basal dendrite of Neuron#1.
for a=0, (basalSize-1){  //For every point from the basal dendrite of
Neuron #1
r3  =  sqrt(x_dend^2+(abs(n2-ii)*x_soma)^2+(basalX.x[a]*Lbasal+Lsoma/2)^2)
//
```

```
denominator3 = 4*PI *r3/rhoa
Ve_basal2soma_n2[a]=new Vector(i_basal_n1[neuron2][a].size())
Ve_basal2soma_n2[a]=i_basal_n1[neuron2][a].c
Ve_basal2soma_n2[a].mul(factor*10^4/denominator3)

Ve_n2_soma[ib].add(Ve_basal2soma_n2[a])
}


}

//-------------------------------------------------------------------------
-------
//This section is to calculate the extracellular voltages applied to
the basal dendrite of Neuron #2
//-------------------------------------------------------------------------
-------

for ic=0, (basalSize-1){ //For each point on the basal dendrite of
Neuron #2



                // For each point on the soma of Neuron#2,
                //the extracellular voltage should be the sum of all
of the extracellular voltages calculated
                //from the apical dendrite, soma, and basal dendrite
(superposition).

       //Calculate the corresponding extracellular voltages on basal
dendrite of Neuron#2
       //from apical dendrites of Neuron#1.

// *****
j=0 k=0 a=0
for j=0, (apicalSize-1){ //For every point from the apical Dendrite of
Neuron #1

r1 = sqrt(x_dend^2+(abs(n2-
ii)*x_soma)^2+(apicalX.x[j]*Lapical+Lsoma+basalX.x[ic]*Lbasal)^2)
//When the point on Neuron#1 is positioned higher than the point on
Neuron#2
denominator1= 4* PI*r1/rhoa
Ve_apical2basal_n2[j] = new Vector(i_apical_n1[neuron2][j].size())
Ve_apical2basal_n2[j]=i_apical_n1[neuron2][j].c
Ve_apical2basal_n2[j].mul(factor*10^4/denominator1)

//Add the extracelluar voltage got from this specific point on Neuron#1
into the i point of Neuron #2
Ve_n2_basal[ic].add(Ve_apical2basal_n2[j])
}

// *****
```

```
//Calculate the corresponding extracellular voltages onto the basal
dendrite of Neuron#2
//from soma of Neuron#1.

for k=0, (somaSize-1){  //For every point from the soma of Neuron #1

r2 = sqrt(x_dend^2+(abs(n2-
ii)*x_soma)^2+(Lsoma/2+basalX.x[ic]*Lbasal)^2)
denominator2 = 4*PI*r2/rhoa
Ve_soma2basal_n2[k]=new Vector(i_soma_n1[neuron2][k].size())
Ve_soma2basal_n2[k]=i_soma_n1[neuron2][k].c
Ve_soma2basal_n2[k].mul(factor*10^4/denominator2)

Ve_n2_basal[ic].add(Ve_soma2basal_n2[k])
}
// *****

//Calculate the corresponding extracellular voltages on basal dendrite
of Neuron#2
//from basal dendrite of Neuron#1.
for a=0, (basalSize-1){  //For every point from the basal dendrite of
Neuron #1

r3 = sqrt(x_dend^2+(abs(n2-ii)*x_soma)^2+((abs(basalX.x[ic]-
basalX.x[a]))*Lbasal)^2)


denominator3 = 4*PI *r3/rhoa
Ve_basal2basal_n2[a]=new Vector(i_basal_n1[neuron2][a].size())
Ve_basal2basal_n2[a]=i_basal_n1[neuron2][a].c
Ve_basal2basal_n2[a].mul(factor*10^4/denominator3)

Ve_n2_basal[ic].add(Ve_basal2basal_n2[a])
}

}
}


////////////////////////////////////////////////////////////////
print "We are printing the size:"
print Ve_n2_apical[0].size()
```

A.4 Single cell layer field recording

Script written by Chen Qiu in 2013/1

```
n2=5
n=10

load_file("nrngui.hoc")
```

```
load_file("myCell3d.hoc")


tstop = 1000
dt=0.005
num = tstop/dt +1
print "num is ", num


objref tvec
tvec = new Vector(num)
tvec.indgen(0,tstop,dt)
//print "tvec size", tvec.size()

load_file("readData3-4Current.hoc")
SecondNeuronRow=4
FirstNeuronRow=3

objref randDistance, f1
f1=new File()
f1.ropen("randDistance.txt")
newNum = f1.scanvar()
printf("Our new num is %d\n", newNum)
//print randDistance.x[0]
objref r
r=new Random(newNum)

load_file("meanD.hoc")

r.normal(meanD,0.1)
randomD=r.repick()+30
print "randomD=", randomD


load_file("xtraVoltage2-3.hoc")
print "finish readData3-4"

////////////////////////////////////////////////////////////////////
load_file("shiftRow3.hoc")

//Apply ephaptic effect stimulation

proc setStimApical(){
apical[0]{

j=0
for (x,0){
Ve_n3_apical[j].play(&e_extracellular(x),tvec)

//print "Apical x= ",x, " ", x*Lapical, " um"
j=j+1
}
}
}
```

```
proc setStimSoma() {
soma{
for (x,0){
Ve_n3_soma[0].play(&e_extracellular(x),tvec)

//print "Soma x= ",x," ", x*8.9, " um"
}
}
}


proc setStimBasal(){
basal[0]{
z=0
for (x,0){
Ve_n3_basal[z].play(&e_extracellular(x),tvec)

//print "Basal x= ", x, " ", x*Lbasal, " um"
z=z+1
}

}
}

setStimApical()
setStimSoma()
setStimBasal()

////////////////////////////////////////////////////////////////////
////////////////////////////////

load_file("record.hoc")
//load_file("neuron2-1.ses")


init()
run()

 //////////////////Plotting the Field//////////////////////////
objref ga,gb, gc, field1, field2, avgField
/*
ga=new Graph()
Ve_n3_apical[10].plot(ga,dt,3,2) //blue
Ve_n3_soma[0].plot(ga,dt,2,2)//Red
Ve_n3_basal[5].plot(ga,dt,4,2)//Green
*/

field1=new Vector()
field2=new Vector()
avgField=new Vector()

field1=Ve_n3_apical[10].c
field1.sub(Ve_n3_soma[0])
```

```
field1.mul(10^3/(apicalX.x[10]*Lapical+0.5*Lsoma))

print "apicaldistance= ",apicalX.x[10]*Lapical+0.5*Lsoma, " um."

print "Field1=(Vtop-Vmiddle)/distance; max= ", field1.max(), "mV/mm;
min= ", field1.min(), " mV/mm"

field2=Ve_n3_basal[5].c
field2.sub(Ve_n3_soma[0])
field2.mul(10^3/(basalX.x[5]*Lbasal+0.5*Lsoma))

field2=Ve_n3_basal[5].c
field2.sub(Ve_n3_soma[0])

avgField=field1.c
avgField.add(field2)
avgField.mul(0.5)

objref f4
f4=new File()
f4.wopen("field3-4.txt")
avgField.vwrite(f4)

print "basaldistance= ",basalX.x[5]*Lbasal+0.5*Lsoma, " um."

print "Field2=(Vbottom-Vmiddle)/distance; max= ", field2.max(), "mV/mm;
min= ", field2.min(), " mV/mm"

print "Average Field= ", avgField.max(), "mV/mm."
print "avgField size= ", avgField.size()


print "Factor= ", factor



objref outputFile
outputFile=new File()
outputFile.aopen("neuronRow3-4Field.txt")
outputFile.printf("%f ", randomD)
outputFile.printf("%f ",field1.max())
outputFile.printf("%f \n",field2.max())
outputFile.flush()

////////////////////////////////////////////////////////////
index1=vm_3.max_ind(470/dt,510/dt)
print  "Neuron C-", n2,"peak 1=", index1*dt

objref f1, f2, f3
f1 = new File()
f2 = new File()
f3 = new File()
f1.wopen("somaCurrent4-5.txt")
f2.wopen("apicalCurrent4-5.txt")
```

```
f3.wopen("basalCurrent4-5.txt")

load_file("processData.hoc")

strdef baseName
baseName = "exV_rowC_neuron"
load_file("recordExV.hoc")

gb=new Graph()
gc=new Graph()

field1.mul(-1)
field2.mul(-1)
avgField.mul(-1)

field1.plot(gb,dt,3,2)//blue
field2.plot(gb,dt,2,2)//red
avgField.plot(gc,dt,3,2)//blue Average Field

print "finish NeuronD-", n2
```

Bibliography

[1] A. Kumar, S. Rotter, and A. Aertsen, “Spiking activity propagation in neuronal networks: reconciling different perspectives on neural coding,” *Nat. Rev. Neurosci.*, vol. 11, no. 9, pp. 615–627, Sep. 2010.

[2] J. H. McAuley and C. D. Marsden, “Physiological and pathological tremors and rhythmic central motor control,” *Brain*, vol. 123, no. 8, pp. 1545–1567, Aug. 2000.

[3] V. Shusterman and W. C. Troy, “From baseline to epileptiform activity: a path to synchronized rhythmicity in large-scale neural networks,” *Phys. Rev. E Stat. Nonlin. Soft Matter Phys.*, vol. 77, no. 6 Pt 1, p. 061911, Jun. 2008.

[4] J. R. Gibson, M. Beierlein, and B. W. Connors, “Functional Properties of Electrical Synapses Between Inhibitory Interneurons of Neocortical Layer 4,” *J. Neurophysiol.*, vol. 93, no. 1, pp. 467–480, Aug. 2004.

[5] A. Konnerth, U. Heinemann, and Y. Yaari, “Nonsynaptic epileptogenesis in the mammalian hippocampus in vitro. I. Development of seizurelike activity in low extracellular calcium,” *J. Neurophysiol.*, vol. 56, no. 2, pp. 409–423, Aug. 1986.

[6] F. Weissinger, K. Buchheim, H. Siegmund, U. Heinemann, and H. Meierkord, “Optical imaging reveals characteristic seizure onsets, spread patterns, and propagation velocities in hippocampal-entorhinal cortex slices of juvenile rats,” *Neurobiol. Dis.*, vol. 7, no. 4, pp. 286–298, Aug. 2000.

[7] J. Lian, M. Bikson, J. Shuai, and D. M. Durand, “Propagation of non-synaptic epileptiform activity across a lesion in rat hippocampal slices,” *J. Physiol.*, vol. 537, no. Pt 1, pp. 191–199, Nov. 2001.

[8] D. M. Durand, E.-H. Park, and A. L. Jensen, “Potassium diffusive coupling in neural networks,” *Philos. Trans. R. Soc. B Biol. Sci.*, vol. 365, no. 1551, pp. 2347–2362, Jul. 2010.

[9] K. Bar-Eli, “Coupling of chemical oscillators,” *J. Phys. Chem.*, vol. 88, no. 16, pp. 3616–3622, Aug. 1984.

[10] C. A. Anastassiou, R. Perin, H. Markram, and C. Koch, “Ephaptic coupling of cortical neurons,” *Nat. Neurosci.*, vol. 14, no. 2, pp. 217–223, Jan. 2011.

[11] B. Katz and O. H. Schmitt, “Electric interaction between two adjacent nerve fibres,” *J. Physiol.*, vol. 97, no. 4, pp. 471–488, Feb. 1940.

[12] H. Bokil, N. Laaris, K. Blinder, M. Ennis, and A. Keller, “Ephaptic interactions in the mammalian olfactory system,” *J. Neurosci. Off. J. Soc. Neurosci.*, vol. 21, no. 20, p. RC173, Oct. 2001.

[13] M. Kamermans and I. Fahrenfort, “Ephaptic interactions within a chemical synapse: hemichannel-mediated ephaptic inhibition in the retina,” *Curr. Opin. Neurobiol.*, vol. 14, no. 5, pp. 531–541, Oct. 2004.

[14] D. S. Faber and H. Korn, “Electrical field effects: their relevance in central neural networks,” *Physiol. Rev.*, vol. 69, no. 3, pp. 821–863, Jul. 1989.

[15] T. Radman, Y. Su, J. H. An, L. C. Parra, and M. Bikson, “Spike timing amplifies the effect of electric fields on neurons: implications for endogenous field effects,” *J. Neurosci. Off. J. Soc. Neurosci.*, vol. 27, no. 11, pp. 3030–3036, Mar. 2007.

[16] H. Korn and H. Axelrad, “Electrical inhibition of Purkinje cells in the cerebellum of the rat,” *Proc Natl Acad Sci USA*, vol. 77, no. 10, pp. 6244–6247, Oct. 1980.

[17] J. T. Francis, B. J. Gluckman, and S. J. Schiff, “Sensitivity of neurons to weak electric fields,” *J. Neurosci. Off. J. Soc. Neurosci.*, vol. 23, no. 19, pp. 7255–7261, Aug. 2003.

[18] E. V. Lubenov and A. G. Siapas, “Hippocampal theta oscillations are travelling waves,” *Nature*, vol. 459, no. 7246, pp. 534–539, May 2009.

[19] A. B. Kibler and D. M. Durand, “Orthogonal wave propagation of epileptiform activity in the planar mouse hippocampus in vitro,” *Epilepsia*, vol. 52, no. 9, pp. 1590–1600, Sep. 2011.

[20] R. Miles, R. D. Traub, and R. K. Wong, “Spread of synchronous firing in longitudinal slices from the CA3 region of the hippocampus,” *J. Neurophysiol.*, vol. 60, no. 4, pp. 1481–1496, Oct. 1988.

[21] J.-S. Liu, J.-B. Li, X.-W. Gong, H.-Q. Gong, P.-M. Zhang, P.-J. Liang, and Q.-C. Lu, “Spatiotemporal dynamics of high-K+-induced epileptiform discharges in hippocampal slice and the effects of valproate,” *Neurosci. Bull.*, vol. 29, no. 1, pp. 28–36, Feb. 2013.

[22] P. P. Quilichini, D. Diabira, C. Chiron, Y. Ben-Ari, and H. Gozlan, “Persistent epileptiform activity induced by low Mg2+ in intact immature brain structures,” *Eur. J. Neurosci.*, vol. 16, no. 5, pp. 850–860, Sep. 2002.

[23] H. L. Haas and J. G. Jefferys, “Low-calcium field burst discharges of CA1 pyramidal neurones in rat hippocampal slices,” *J. Physiol.*, vol. 354, pp. 185–201, Sep. 1984.

[24] N. L. M. Cappaert, F. H. Lopes da Silva, and W. J. Wadman, “Spatio-temporal dynamics of theta oscillations in hippocampal-entorhinal slices,” *Hippocampus*, vol. 19, no. 11, pp. 1065–1077, Nov. 2009.

[25] M. Bikson, R. S. Ghai, S. C. Baraban, and D. M. Durand, “Modulation of burst frequency, duration, and amplitude in the zero-Ca(2+) model of epileptiform activity,” *J. Neurophysiol.*, vol. 82, no. 5, pp. 2262–2270, Nov. 1999.

[26] M. Zhang, T. P. Ladas, C. Qiu, R. S. Shivacharan, L. E. Gonzalez-Reyes, and D. M. Durand, "Propagation of epileptiform activity can be independent of synaptic transmission, gap junctions, or diffusion and is consistent with electrical field transmission," *J. Neurosci. Off. J. Soc. Neurosci.*, vol. 34, no. 4, pp. 1409–1419, Jan. 2014.

[27] J. P. Meeks and S. Mennerick, "Action potential initiation and propagation in CA3 pyramidal axons," *J. Neurophysiol.*, vol. 97, no. 5, pp. 3460–3472, May 2007.

[28] A. L. Jensen, "Control of Axonal Conduction of High Frequency Stimulation," Case Western Reserve University, 2008.

[29] F. Fröhlich and D. A. McCormick, "Endogenous Electric Fields May Guide Neocortical Network Activity," *Neuron*, vol. 67, no. 1, pp. 129–143, Jul. 2010.

[30] E. J. Vigmond, J. L. Perez Velazquez, T. A. Valiante, B. L. Bardakjian, and P. L. Carlen, "Mechanisms of electrical coupling between pyramidal cells," *J. Neurophysiol.*, vol. 78, no. 6, pp. 3107–3116, Dec. 1997.

[31] J. Shuai, M. Bikson, P. J. Hahn, J. Lian, and D. M. Durand, "Ionic mechanisms underlying spontaneous CA1 neuronal firing in Ca2+-free solution," *Biophys. J.*, vol. 84, no. 3, pp. 2099–2111, Mar. 2003.

[32] E. N. Warman, D. M. Durand, and G. L. Yuen, "Reconstruction of hippocampal CA1 pyramidal cell electrophysiology by computer simulation," *J. Neurophysiol.*, vol. 71, no. 6, pp. 2033–2045, Jun. 1994.

[33] M. A. Kurt, M. I. Kafa, M. Dierssen, and D. C. Davies, "Deficits of neuronal density in CA1 and synaptic density in the dentate gyrus, CA3 and CA1, in a mouse model of Down syndrome," *Brain Res.*, vol. 1022, no. 1–2, pp. 101–109, Oct. 2004.

[34] A. L. Hodgkin and A. F. Huxley, "A quantitative description of membrane current and its application to conduction and excitation in nerve," *J. Physiol.*, vol. 117, no. 4, pp. 500–544, Aug. 1952.

[35] S. Jinno and T. Kosaka, "Stereological estimation of numerical densities of glutamatergic principal neurons in the mouse hippocampus," *Hippocampus*, vol. 20, no. 7, pp. 829–840, Jul. 2010.

[36] A. B. Kibler, B. G. Jamieson, and D. M. Durand, "A high aspect ratio microelectrode array for mapping neural activity in vitro," *J. Neurosci. Methods*, vol. 204, no. 2, pp. 296–305, Mar. 2012.

[37] P. Perreault and M. Avoli, "Effects of low concentrations of 4-aminopyridine on CA1 pyramidal cells of the hippocampus," *J. Neurophysiol.*, vol. 61, no. 5, pp. 953–970, May 1989.

[38] P. Perreault and M. Avoli, "4-aminopyridine-induced epileptiform activity and a GABA-mediated long-lasting depolarization in the rat hippocampus," *J. Neurosci. Off. J. Soc. Neurosci.*, vol. 12, no. 1, pp. 104–115, Jan. 1992.

[39] L. E. Schechter, “The potassium channel blockers 4-aminopyridine and tetraethylammonium increase the spontaneous basal release of [3H]5-hydroxytryptamine in rat hippocampal slices,” *J. Pharmacol. Exp. Ther.*, vol. 282, no. 1, pp. 262–270, Jul. 1997.

[40] B. He, “Electrical stimulation of the neuromuscular system,” in *Neural Engineering*, 2005th ed., vol. 3, Springer, 2005, p. 503.

[41] C. Gold, D. A. Henze, and C. Koch, “Using extracellular action potential recordings to constrain compartmental models,” *J. Comput. Neurosci.*, vol. 23, no. 1, pp. 39–58, Aug. 2007.

[42] N. K. Logothetis, C. Kayser, and A. Oeltermann, “In vivo measurement of cortical impedance spectrum in monkeys: implications for signal propagation,” *Neuron*, vol. 55, no. 5, pp. 809–823, Sep. 2007.

[43] A. Schmoldt, H. F. Benthe, and G. Haberland, “Digitoxin metabolism by rat liver microsomes,” *Biochem. Pharmacol.*, vol. 24, no. 17, pp. 1639–1641, Sep. 1975.

[44] M. L. Ledbetter and R. D. Hotchkiss, “Chromosomal basis of the merozygosity in a partially deploid mutant of Pneumococcus,” *Genetics*, vol. 80, no. 4, pp. 667–678, Aug. 1975.

[45] A. N. Klimov, A. A. Nikiforova, V. T. Lozovskiĭ, A. M. Chistiakova, and E. I. Magracheva, “[HDL2c--a new subclass of high density lipoproteins in the plasma of newborns],” *Biokhimiia Mosc. Russ.*, vol. 43, no. 9, pp. 1721–1722, Sep. 1978.

[46] A. B. Makar, K. E. McMartin, M. Palese, and T. R. Tephly, “Formate assay in body fluids: application in methanol poisoning,” *Biochem. Med.*, vol. 13, no. 2, pp. 117–126, Jun. 1975.

[47] H. Su, G. Alroy, E. D. Kirson, and Y. Yaari, “Extracellular calcium modulates persistent sodium current-dependent burst-firing in hippocampal pyramidal neurons,” *J. Neurosci. Off. J. Soc. Neurosci.*, vol. 21, no. 12, pp. 4173–4182, Jun. 2001.

[48] D. Golomb, C. Yue, and Y. Yaari, “Contribution of persistent Na+ current and M-type K+ current to somatic bursting in CA1 pyramidal cells: combined experimental and modeling study,” *J. Neurophysiol.*, vol. 96, no. 4, pp. 1912–1926, Oct. 2006.

[49] R. S. Ghai, M. Bikson, and D. M. Durand, “Effects of applied electric fields on low-calcium epileptiform activity in the CA1 region of rat hippocampal slices,” *J. Neurophysiol.*, vol. 84, no. 1, pp. 274–280, Jul. 2000.

[50] J. Deuchars and A. M. Thomson, “CA1 pyramid-pyramid connections in rat hippocampus in vitro: dual intracellular recordings with biocytin filling,” *Neuroscience*, vol. 74, no. 4, pp. 1009–1018, Oct. 1996.

[51] V. C. Wimmer, C. A. Reid, S. Mitchell, K. L. Richards, B. B. Scaf, B. T. Leaw, E. L. Hill, M. Royeck, M.-T. Horstmann, B. A. Cromer, P. J. Davies, R. Xu, H. Lerche, S. F. Berkovic, H. Beck, and S. Petrou, “Axon initial segment dysfunction in a mouse

model of genetic epilepsy with febrile seizures plus," *J. Clin. Invest.*, vol. 120, no. 8, pp. 2661–2671, Aug. 2010.

[52] E. Shahar, M. Derchansky, and P. L. Carlen, "The role of altered tissue osmolality on the characteristics and propagation of seizure activity in the intact isolated mouse hippocampus," *Clin. Neurophysiol. Off. J. Int. Fed. Clin. Neurophysiol.*, vol. 120, no. 4, pp. 673–678, Apr. 2009.

[53] C. Y. Chan and C. Nicholson, "Modulation by applied electric fields of Purkinje and stellate cell activity in the isolated turtle cerebellum," *J. Physiol.*, vol. 371, pp. 89–114, Feb. 1986.